# THE DYNAMICS OF DISCRETE FACT

*A Phase-Transition Theory of Wavefunction Collapse*

**Ahmed Hamid Mahmoud**
King Fahd University of Petroleum and Minerals, Dhahran, Saudi Arabia
ahmed.hamid@kfupm.edu.sa

February 2026

**Abstract**

The quantum measurement problem—the absence of any dynamical mechanism connecting continuous wavefunction evolution to discrete empirical outcomes—has persisted since the foundations of quantum theory. Decoherence explains interference suppression but cannot explain outcome selection: the diagonal density matrix remains an improper mixture until one outcome is actualized. We propose that collapse is a **physical phase transition** in the coupled system–apparatus field. The order parameter $\psi$, constructed as a conditional collective coordinate of apparatus degrees of freedom, evolves under time-dependent Ginzburg–Landau (TDGL) dynamics with a symmetry-breaking potential. When the coherence pressure $\gamma \equiv g\sqrt{N}|\langle\hat{S}\rangle|/\hbar\omega_S$ exceeds a critical threshold $\gamma_c = \lambda/\hbar\omega_S$, the symmetric phase (superposition) becomes unstable and the field crystallizes into one of the discrete stable minima (eigenstates). We derive the critical coupling from microscopic system–apparatus Hamiltonians, obtaining the scaling $g_c \sim N^{-1/2}$, which explains why macroscopic apparatus collapse wavefunctions while microscopic interactions preserve coherence. The TDGL dynamics are derived from the microscopic Hamiltonian via the Schwinger–Keldysh path integral, with each step a controlled approximation requiring no modification to the Schrödinger equation. The Born rule $P_n = |c_n|^2$ is preserved through a dynamical selection mechanism: an equal-basin-volume theorem—proved from the permutation symmetry of the apparatus interaction—ensures that attractor basin geometry under probability-conserving Fokker–Planck flow converts quantum amplitudes into outcome probabilities. We characterize the quantum-classical interface via two complementary classicality criteria and identify a four-stage measurement chain (unitary evolution → decoherence → coarse-graining → phase transition) that resolves the Heisenberg cut dynamically. The theory yields four falsifiable predictions absent from standard quantum mechanics: critical slowing near $\gamma_c$, hysteresis in the collapse–recoherence cycle, metastable supercooled superpositions, and transient Jacobian spikes at the moment of collapse. Quantitative estimates are provided for three experimental platforms—superconducting transmon readout, cavity QED with Rydberg atoms, and optomechanical systems—with explicit falsification criteria. This framework provides a concrete existence proof that collapse dynamics can be constructed from standard quantum mechanics plus statistical mechanics.

**Keywords:** quantum measurement problem · wavefunction collapse · phase transitions · Ginzburg–Landau theory · Born rule · quantum-classical boundary · spontaneous symmetry breaking

# 1 Introduction

The quantum formalism remains predictively successful but lacks a dynamical mechanism for state reduction. The Schrödinger equation

$$i\hbar\frac{\partial}{\partial t}|\Psi(t)\rangle = \hat{H}|\Psi(t)\rangle \tag{1}$$

describes a continuous, deterministic, and reversible evolution of the state vector through Hilbert space $\mathscr{H}$. Yet every act of observation yields not a superposition but a *single eigenvalue*—discrete, irreversible, and stochastic. The standard formalism bridges this chasm with the projection postulate

$$|\Psi\rangle \longrightarrow \frac{\hat{P}_n|\Psi\rangle}{\sqrt{\langle\Psi|\hat{P}_n|\Psi\rangle}}, \tag{2}$$

where $\hat{P}_n = |a_n\rangle\langle a_n|$ projects onto the observed eigenstate [1]. This postulate specifies *that* the transition occurs but remains silent on *how*, *when*, or *why*—it is prescription, not dynamics.

This silence is not a minor gap but a foundational one. As Bell articulated, the measurement postulate introduces into fundamental physics a concept—"measurement"—that presupposes the very macroscopic definiteness it purports to explain [2]. The formalism thus contains a logical circularity at its core, what we shall term the **Transition Problem**: the absence of any dynamical mechanism connecting the continuous evolution of probability amplitudes to the discrete emergence of empirical facts.

## 1.1 The Inadequacy of Decoherence

Environmental decoherence has been advanced as the resolution to this impasse [3, 4]. When a quantum system $\mathscr{S}$ couples to an environment $\mathscr{E}$, the reduced density matrix $\hat{\rho}_{\mathscr{S}} = \mathrm{Tr}_{\mathscr{E}}[\hat{\rho}_{\mathscr{S}\mathscr{E}}]$ undergoes rapid diagonalization in the pointer basis:

$$\hat{\rho}_{\mathscr{S}}(t) = \sum_{n,m} c_n c_m^* e^{-\Gamma_{nm}t}|a_n\rangle\langle a_m| \xrightarrow{t\gg\tau_D} \sum_n |c_n|^2|a_n\rangle\langle a_n|. \tag{3}$$

This process, while physically genuine, addresses only part of the problem. Decoherence explains the *suppression of interference*—why we do not observe superpositions of macroscopically distinct states. It does *not* explain the *selection of outcomes*—why one particular $|a_n\rangle$ is actualized rather than another. The diagonal density matrix (3) represents an improper mixture, epistemically equivalent to classical ignorance only if exactly one outcome *already* obtains. Decoherence thus presupposes the very actualization it claims to derive.

This logical structure—the "and-to-or" transition problem [5]—admits no solution within unitary quantum mechanics. The trace over environmental degrees of freedom cannot convert a pure-state superposition into a single definite outcome;

it can only render the superposition *observationally inaccessible*. The measurement problem remains.

### 1.2 The Thesis of This Work

We propose that collapse is neither a postulate nor an illusion but a **physical phase transition** in the coupled system–apparatus field. Just as ferromagnetic ordering emerges when thermal fluctuations fall below a critical threshold, eigenstate definiteness emerges when coherence constraints exceed a critical coupling. The mechanism is *spontaneous symmetry breaking*: the potential landscape of the coupled field transforms from a single symmetric minimum (superposition) to multiple asymmetric minima (eigenstates), and the field must "choose" one.

This framework is dynamical rather than interpretive: it yields quantitative predictions absent from standard quantum mechanics, distinguishing it empirically from Copenhagen, Many-Worlds, and objective-collapse theories. We derive the critical coupling from microscopic Hamiltonians, compute the scaling exponents governing collapse dynamics, and identify experimental signatures—including critical slowing, hysteresis, and metastable quantum states—that admit direct laboratory test.

## 2 The Measurement Problem

Before constructing the dynamical solution, we must analyze the problem carefully. The measurement problem is not one problem but three interlocking puzzles [6, 7], each requiring distinct theoretical machinery.

### 2.1 The Problem of Outcomes (Definiteness)

Quantum mechanics assigns to every observable $\hat{A}$ a complete orthonormal basis $\{|a_n\rangle\}$ of eigenstates [8]. A general state $|\Psi\rangle = \sum_n c_n |a_n\rangle$ encodes all possible outcomes simultaneously. Yet experiment yields exactly one. What produces this definiteness?

The formal structure of the problem is as follows. Define the "actualization map" $\mathscr{A} : \mathscr{H} \to \{|a_n\rangle\}$ that takes superpositions to eigenstates. This map must satisfy:

1. **Stochasticity**: $\mathscr{A}$ is not deterministic; $\text{Prob}(\mathscr{A}[|\Psi\rangle] = |a_n\rangle) = |c_n|^2$.
2. **Idempotence**: $\mathscr{A}[|a_n\rangle] = |a_n\rangle$ (eigenstates are fixed points).
3. **Irreversibility**: $\mathscr{A}^{-1}$ does not exist as a physical process.

No unitary operator satisfies these conditions. Unitarity preserves inner products and is invertible; $\mathscr{A}$ violates both. The measurement problem, at its mathematical core, is the demand for a *non-unitary* map within a theory whose fundamental dynamics are purely unitary.

### 2.2 The Problem of Preferred Basis (Selection)

Even granting that superpositions collapse, *which* basis? The state $|\Psi\rangle$ admits infinitely many decompositions into orthonormal sets. The position basis, momentum basis, and energy basis are all mathematically equivalent. Yet nature selects: spin measurements yield spin eigenstates, position measurements yield (approximate) position eigenstates.

This basis selection cannot emerge from the system alone—it requires the apparatus. The apparatus Hamiltonian $\hat{H}_A$ and the interaction Hamiltonian $\hat{H}_{SA}$ together define a *pointer basis* through the einselection mechanism [3]. But einselection, like decoherence, is necessary not sufficient. It explains which basis is stable against environmental monitoring; it does not explain why one basis element is actualized.

### 2.3 The Problem of the Cut (Demarcation)

Where does quantum end and classical begin? Von Neumann demonstrated that the "cut" between system and apparatus can be placed at any point in the measurement chain without altering predictions—the "von Neumann chain" [1, 7]. But *some* cut must exist, for we observe definite outcomes. The arbitrariness of the formal cut conceals a real physical transition.

We propose that this transition is not arbitrary but **dynamically determined**. The cut occurs where the coherence pressure $\gamma$ first exceeds the critical value $\gamma_c$. This is calculable from the physical parameters of the apparatus, resolving the demarcation problem quantitatively.

## 3 Phase Transitions as Generators of Discrete Structure

The conceptual key to our theory lies in recognizing that nature already possesses a mechanism for generating discrete, stable structures from continuous dynamics: the phase transition. We here develop the relevant formalism in sufficient generality to encompass both thermodynamic and quantum applications.

### 3.1 The Landau Paradigm

Landau's theory of phase transitions [9] rests on a key insight: near a critical point, the free energy $\mathscr{F}$ can be expanded as a functional of an *order parameter* $\psi$ that quantifies the degree of symmetry breaking:

$$\mathscr{F}[\psi] = \int d^d x \left[ \frac{1}{2}|\nabla\psi|^2 + \frac{\alpha}{2}|\psi|^2 + \frac{\beta}{4}|\psi|^4 + \cdots \right]. \quad (4)$$

The control parameter $\alpha$ determines the phase structure:

- $\alpha > 0$: Single minimum at $\psi = 0$ (symmetric phase).
- $\alpha < 0$: Ring of minima at $|\psi| = \sqrt{-\alpha/\beta}$ (broken-symmetry phase).

At $\alpha = 0$, the system undergoes a phase transition. The symmetric configuration becomes unstable, and the field *must* select one of the equivalent minima—spontaneous symmetry breaking.

### 3.2 Energetic Stability and Macroscopic Rigidity

Once the system occupies a broken-symmetry minimum, it is **energetically stable**. Transitions between degenerate minima require either (i) thermal fluctuations sufficient to surmount the energy barrier $\Delta E = \mathscr{F}[\psi = 0] - \mathscr{F}[\psi_{\min}]$, or (ii) coherent tunneling through the barrier. For macroscopic systems, both are exponentially suppressed:

$$\Gamma_{\text{transition}} \sim e^{-\Delta E/k_B T} \quad \text{or} \quad e^{-S_{\text{instanton}}/\hbar}, \tag{5}$$

where $S_{\text{instanton}}$ is the Euclidean action of the tunneling path.

This exponential stability is the physical origin of *definiteness*—the robustness of actualized outcomes against small perturbations. An eigenstate, once selected, persists not by postulate but by energetic protection.

### 3.3 Critical Phenomena and Universality

Near the critical point, physical quantities exhibit power-law scaling governed by *universal* critical exponents:

$$\xi \sim |\alpha - \alpha_c|^{-\nu} \qquad \text{(correlation length)}, \tag{6}$$

$$\chi \sim |\alpha - \alpha_c|^{-\gamma_{\text{exp}}} \qquad \text{(susceptibility)}, \tag{7}$$

$$\tau \sim \xi^z \sim |\alpha - \alpha_c|^{-\nu z} \qquad \text{(relaxation time)}. \tag{8}$$

The exponents $\nu$, $\gamma_{\text{exp}}$, $z$ depend only on dimensionality and symmetry class, not microscopic details—universality [10]. This universality will prove essential: it implies that quantum collapse, if indeed a phase transition, must exhibit the same scaling behavior regardless of the specific apparatus employed.

### 3.4 Why Measurement Falls in the Ising Universality Class

The application of Ginzburg–Landau theory [11] to quantum measurement requires justification beyond analogy. We here provide the physical intuition; a rigorous derivation from first principles appears in Section 5.

The key observation is that measurement outcomes are **discrete**. A spin-1/2 measurement yields $\pm\hbar/2$, not a continuous spectrum. This discreteness implies a **discrete symmetry** in the order parameter space. For a two-outcome measurement, the symmetry is $\mathbb{Z}_2$: the potential must be invariant under $\psi \to -\psi$.

Given this symmetry constraint, the effective potential must satisfy $V(\psi) = V(-\psi)$. Expanding in powers of $\psi$:

$$V(\psi) = a_0 + a_2\psi^2 + a_4\psi^4 + \mathscr{O}(\psi^6). \tag{9}$$

Odd powers are forbidden by symmetry. The $\psi^4$ term is the leading nonlinearity. Higher-order terms ($\psi^6$, $\psi^8$, ...) are irrelevant in the renormalization group sense in the mean-field regime ($d_{\text{eff}} > 4$, cf. Appendix D), as their scaling dimensions are positive [10]. The $\phi^4$ theory therefore constitutes the *minimal* effective description near criticality.

Therefore, *any* measurement apparatus with two discrete outcomes, subject to locality and coarse-graining, must be described by a $\phi^4$ effective theory near the critical regime. The Landau potential (19) is not an ad hoc choice but the **minimal effective theory** consistent with the stated symmetry and RG constraints. Section 5 demonstrates this and exhibits a canonical representative model (the Curie–Weiss pointer) for which the derivation is fully explicit.

For $n$-outcome measurements, the symmetry generalizes to $\mathbb{Z}_n$ or permutation groups, leading to more complex potentials with $n$ degenerate minima. The qualitative physics—symmetry breaking, basin structure, critical dynamics—remains identical.

## 4 The Coupled System–Apparatus Field

We now construct the field-theoretic description of the combined quantum system and measuring apparatus whose dynamics naturally incorporate both unitary evolution and symmetry-breaking collapse.

### 4.1 Microscopic Foundation: The System–Apparatus Hamiltonian

We begin not with postulates but with the standard quantum mechanical description of measurement. Consider a system $\mathscr{S}$ with Hilbert space $\mathscr{H}_S$ coupled to an apparatus $\mathscr{A}$ consisting of $N$ microscopic degrees of freedom. The total Hamiltonian is

$$\hat{H} = \hat{H}_S + \hat{H}_A + \hat{H}_{\text{int}}, \tag{10}$$

where the interaction takes the form

$$\hat{H}_{\text{int}} = g \sum_{i=1}^{N} \hat{S} \otimes \hat{A}_i. \tag{11}$$

Here $\hat{S}$ is the system observable being measured, $\hat{A}_i$ are apparatus operators (e.g., spin components, phonon modes, or photon field amplitudes), and $g$ is the microscopic coupling constant.

### 4.2 Construction of the Order Parameter

The order parameter $\psi$ is **not** a new fundamental field but emerges from the *conditional* wavefunction of the apparatus given a particular measurement branch. This conditional construction is essential: symmetry breaking occurs not in the ensemble-averaged pointer, but in the dynamics of each branch individually.

**Conditional construction.** Consider the full quantum state of the system–apparatus composite:

$$|\Psi(t)\rangle = \sum_n c_n |a_n\rangle \otimes |\phi_n(t)\rangle, \tag{12}$$

where $\{|a_n\rangle\}$ are the eigenstates of the measured observable and $|\phi_n(t)\rangle$ are the corresponding apparatus states, initially identical but driven apart by the measurement interaction. Under environmental monitoring (premise D), the apparatus states decohere on a timescale $\tau_D$:

$$\langle \phi_m(t) | \phi_n(t) \rangle \to \delta_{mn} \quad \text{for } t \gg \tau_D. \tag{13}$$

We define the *conditional order parameter* for outcome $n$ as the macroscopic pointer position evaluated within the $n$-th apparatus branch:

$$\boxed{\psi_n(t) \equiv \frac{1}{\sqrt{N}} \sum_{i=1}^{N} \langle \phi_n(t) | \hat{A}_i | \phi_n(t) \rangle} \tag{14}$$

The $1/\sqrt{N}$ normalization ensures that $\psi_n$ has well-defined fluctuations in the thermodynamic limit. This is the macroscopic pointer position *conditioned* on the system being in state $|a_n\rangle$. The symmetry breaking of the theory—the passage from a symmetric potential to a definite minimum—occurs in the dynamics of each $\psi_n$, not in an ensemble average.

**Relation to the unconditional collective coordinate.** The quantity used in the main text equations (e.g., Eq. (18)–(19)) should be understood as follows. The unconditional collective coordinate is:

$$\Phi(t) = \mathrm{Tr}\left[\hat{\rho}_A(t)\, \hat{A}_{\mathrm{avg}}\right], \quad \hat{A}_{\mathrm{avg}} \equiv \frac{1}{\sqrt{N}} \sum_{i=1}^{N} \hat{A}_i, \tag{15}$$

where $\hat{\rho}_A(t) = \mathrm{Tr}_S[|\Psi(t)\rangle\langle\Psi(t)|]$ is the reduced apparatus density matrix. This decomposes as:

$$\Phi(t) = \sum_n |c_n|^2\, \psi_n(t), \tag{16}$$

revealing $\Phi$ as the Born-rule-weighted ensemble average of the conditional order parameters. Individual experimental runs correspond to specific $\psi_n$ values; $\Phi$ represents the statistical mixture.

The spatially coarse-grained order parameter is then:

$$\psi(t) = \int d^3x\, f(\mathbf{x})\, \psi_n(\mathbf{x}, t), \tag{17}$$

where $f(\mathbf{x})$ is a smoothing kernel selecting the relevant macroscopic degrees of freedom. The phase transition describes how these conditional values $\psi_n$ become macroscopically definite: each branch evolves under its own effective Ginzburg–Landau dynamics, and the symmetry breaking selects a definite attractor within each conditional trajectory.

**Physical interpretation**: Each $\psi_n$ encodes the macroscopic "pointer position" of the apparatus conditioned on outcome $n$. For a Stern–Gerlach experiment, $\psi_\uparrow$ and $\psi_\downarrow$ represent the two possible center-of-mass positions of the detector screen's response. For a superconducting qubit readout, $\psi_n$ represents the integrated photon field amplitude in the readout resonator conditioned on the qubit being in state $|a_n\rangle$.

**Basis selection**: The measurement basis enters through the *choice* of apparatus operators $\hat{A}_i$ in Eq. (14). These operators are determined by the interaction Hamiltonian $\hat{H}_{\mathrm{int}}$, which couples the system observable $\hat{S}$ to specific apparatus modes. Einselection [3] ensures that only pointer-basis-aligned modes survive environmental monitoring; our framework makes this mechanism explicit by showing that the symmetry of $V(\psi)$—and hence the structure of attractors—is inherited directly from $\hat{H}_{\mathrm{int}}$. Thus, basis selection occurs at the level of $\psi$-construction, not as an additional postulate.

This construction makes explicit that $\psi_n$ and $\Phi$ are **derived quantities**, not fundamental additions to quantum mechanics. They emerge from standard quantum operators via coarse-graining, analogous to how magnetization emerges from atomic spins or how fluid velocity emerges from molecular momenta. Because the transition falls into the Ising universality class, the critical exponents are independent of the specific choice of smoothing kernel $f(\mathbf{x})$.

## 4.3 Emergence of the Ginzburg–Landau Functional

From the microscopic Hamiltonian (10), the effective dynamics of $\psi$ can be derived via standard techniques: integrate out fast degrees of freedom, perform a cumulant expansion, and retain terms to quartic order [12]. The result is an effective free energy functional:

$$\boxed{\mathscr{F}[\psi] = \int d^n x \left[\frac{\kappa}{2}|\nabla\psi|^2 + V(\psi)\right]} \tag{18}$$

where:

- $\kappa > 0$ is the stiffness coefficient penalizing spatial inhomogeneity.
- $V(\psi)$ is the effective potential incorporating the coherence pressure $\gamma$.

For a two-outcome measurement, $\psi \in \mathbb{R}$ and

$$V(\psi) = \frac{\lambda}{2}\left(1 - \frac{\gamma}{\gamma_c}\right)\psi^2 + \frac{\lambda}{4}\psi^4, \tag{19}$$

the standard Landau potential (Fig. 1). When $\gamma < \gamma_c$, the quadratic coefficient is positive and $\psi = 0$ is the unique minimum (symmetric phase, superposition). When $\gamma > \gamma_c$, the quadratic coefficient becomes negative and the potential develops two minima at $\psi = \pm\sqrt{(\gamma/\gamma_c - 1)}$ (broken-symmetry phase, eigenstates).

The coherence pressure $\gamma$ enters the potential through the quadratic coefficient: when $\gamma$ increases (stronger measurement interaction), the effective mass term decreases and eventually changes sign, triggering the phase transition. Table 1 summarizes the principal notation used throughout.

## 4.4 Derivation of the Critical Coupling from Microscopic Parameters

We now derive the critical coupling $\gamma_c$ from the microscopic Hamiltonian. Our starting point is the total Hamiltonian (10)–(11):

$$\hat{H} = \hat{H}_S + \hat{H}_A + g \sum_{i=1}^{N} \hat{S} \otimes \hat{A}_i. \tag{20}$$

The collective coordinate $\Phi$ defined in Eq. (15) has variance

$$\sigma_\Phi^2 = \frac{1}{N} \sum_{i,j} \left(\langle \hat{A}_i \hat{A}_j \rangle - \langle \hat{A}_i \rangle \langle \hat{A}_j \rangle\right). \tag{21}$$

Assuming weak correlations among apparatus modes, cross-terms average to zero, leaving

$$\sigma_\Phi^2 \approx \frac{1}{N} \sum_i \sigma_i^2 \sim \frac{\sigma_0^2}{N}, \tag{22}$$

where $\sigma_0^2$ is the single-mode variance. This is the Central Limit Theorem: collective fluctuations scale as $N^{-1/2}$.

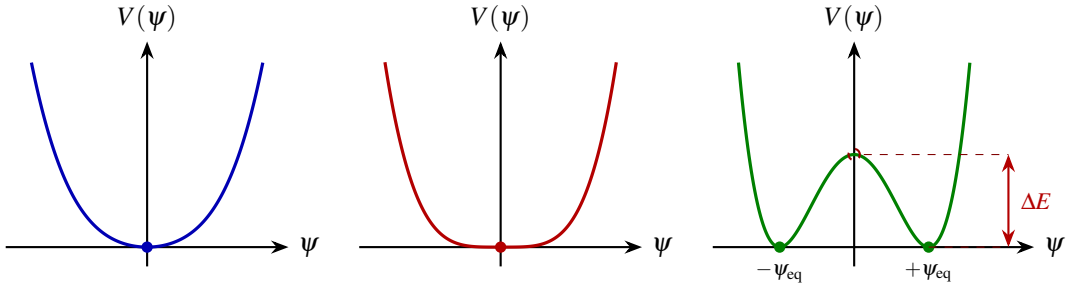


**(a)** $\gamma < \gamma_c$ Symmetric phase (superposition)

**(b)** $\gamma = \gamma_c$ Critical point (marginal)

**(c)** $\gamma > \gamma_c$ Broken symmetry (eigenstates)

Figure 1: **Effective potential $V(\psi)$ as a function of the order parameter $\psi$ for three regimes of the coherence pressure $\gamma$. (a)** For $\gamma < \gamma_c$, the potential has a single minimum at $\psi = 0$ (symmetric phase): the apparatus remains in superposition. **(b)** At $\gamma = \gamma_c$, the quadratic coefficient vanishes and the potential becomes purely quartic—the critical point where fluctuations diverge and collapse time $\tau_c \to \infty$. **(c)** For $\gamma > \gamma_c$, the potential develops two minima at $\psi = \pm\psi_{\rm eq}$ separated by a barrier $\Delta E$: the apparatus must select one of the two eigenstates. Filled circles indicate stable minima; the dashed circle indicates the unstable maximum. The arrows denote the energy barrier whose height controls the irreversibility of the transition.

The effective free energy for the order parameter $\psi$—obtained by integrating out fast degrees of freedom and performing a cumulant expansion—takes the Ginzburg–Landau form (18)–(19):

$$\mathscr{F}[\psi] = \int d^n x \left[\frac{\kappa}{2}|\nabla\psi|^2 + V(\psi)\right],$$
$$V(\psi) = \frac{\lambda}{2}\left(1 - \frac{\gamma}{\gamma_c}\right)\psi^2 + \frac{\lambda}{4}\psi^4. \tag{23}$$

Here $\lambda$ and $\kappa$ are positive constants determined by the apparatus self-interaction and stiffness, respectively. The coherence pressure $\gamma$ encapsulates the measurement strength.

To express $\gamma$ microscopically, we compute the contribution of the interaction Hamiltonian to the effective potential. The interaction energy for a fixed $\psi$ scales as

$$E_{\rm int} \sim g\sqrt{N}\,|\langle\hat{S}\rangle|\,|\psi|, \tag{24}$$

where the factor $\sqrt{N}$ arises because the system couples *coherently* to the collective mode $\Phi$. This $\sqrt{N}$ enhancement is the signature of collective behavior, analogous to superradiance in quantum optics. The apparatus self-energy barrier is set by $\lambda$:

$$\Delta E \sim \lambda. \tag{25}$$

The transition occurs when the interaction energy overcomes the barrier, i.e., when

$$g\sqrt{N}\,|\langle\hat{S}\rangle| \gtrsim \lambda. \tag{26}$$

For a system observable $\hat{S}$ with eigenvalue spectrum $\{s_n\}$, we define the characteristic system frequency:

$$\omega_S \equiv \frac{E_{\max} - E_{\min}}{\hbar} = \frac{s_{\max} - s_{\min}}{\hbar}, \tag{27}$$

where $E_{\max}$ and $E_{\min}$ are the extremal eigenvalues of $\hat{S}$. For a spin-$\frac{1}{2}$ system, $\omega_S = 2s/\hbar$; for a harmonic oscillator truncated at $n$ levels, $\omega_S = n\omega_0$. With this definition, $|\langle\hat{S}\rangle| \le \hbar\omega_S$, and the dimensionless coherence pressure and critical coupling are:

$$\boxed{\gamma \equiv \frac{g\sqrt{N}\,|\langle\hat{S}\rangle|}{\hbar\omega_S}, \qquad \gamma_c \equiv \frac{\lambda}{\hbar\omega_S}} \tag{28}$$

The coherence pressure $\gamma$ is manifestly dimensionless: $g\sqrt{N}$ has units of energy (the collective interaction strength), $|\langle\hat{S}\rangle|$ is the system's expectation value, and $\hbar\omega_S$ is the system's energy scale. When $|\langle\hat{S}\rangle|$ is maximal ($\sim \hbar\omega_S$), the coherence pressure reduces to $\gamma \approx g\sqrt{N}/(\hbar\omega_S)\cdot\hbar\omega_S = g\sqrt{N}$; for partially polarized states, $\gamma$ is reduced by the factor $|\langle\hat{S}\rangle|/(\hbar\omega_S) \le 1$. The critical condition becomes $\gamma/\gamma_c = 1$, i.e.:

$$g\sqrt{N}\,|\langle\hat{S}\rangle| = \lambda. \tag{29}$$

Since $\lambda$ is an apparatus self-energy scale (independent of $N$), we obtain the scaling law

$$\boxed{(g\sqrt{N})_c \sim \text{constant} \implies g_c \sim N^{-1/2}} \tag{30}$$

**Physical Interpretation**: The critical coupling $\gamma_c = \lambda/(\hbar\omega_S)$ is the ratio of the apparatus self-energy to the system energy scale—a property of the apparatus alone. The coherence pressure $\gamma = g\sqrt{N}|\langle\hat{S}\rangle|/(\hbar\omega_S)$ measures the effective measurement strength: the collective coupling $g\sqrt{N}$ enhanced by the system polarization $|\langle\hat{S}\rangle|$, normalized to the system energy scale. The phase transition occurs when $\gamma$ exceeds $\gamma_c$.

**Key Result**: The critical coupling scales as $g_c \sim N^{-1/2}$:

- *Macroscopic apparatus* ($N \sim 10^{23}$): $g_c \sim 10^{-12}$, achievable by even weak interactions.
- *Mesoscopic apparatus* ($N \sim 10^9$): $g_c \sim 10^{-5}$, the regime of current quantum computing experiments.
- *Microscopic "apparatus"* ($N \sim 1$): $g_c \sim 1$, requiring strong coupling to induce collapse.

This scaling law *explains* why macroscopic apparatus ($N \sim 10^{23}$) collapse wavefunctions even with weak coupling, while microscopic systems ($N \sim 1$) require strong coupling to induce a transition. The "classicality" of the apparatus is not a primitive concept but an emergent consequence of the $N^{-1/2}$ scaling.

Table 1: **Summary of principal notation.** All quantities are defined from the microscopic Hamiltonian; none require modifications to standard quantum mechanics.

| Symbol | Name | Definition / meaning |
|---|---|---|
| $\psi_n(t)$ | Conditional order parameter | $\frac{1}{\sqrt{N}}\sum_i \langle\phi_n\|\hat{A}_i\|\phi_n\rangle$ |
| $\Phi(t)$ | Unconditional collective coordinate | $\mathrm{Tr}[\hat{\rho}_A\hat{A}_{\mathrm{avg}}] = \sum_n \|c_n\|^2\psi_n$ |
| $\psi(t)$ | Order parameter (coarse-grained) | $\int d^3x\, f(\mathbf{x})\,\psi_n(\mathbf{x},t)$ |
| $\gamma$ | Coherence pressure | $g\sqrt{N}\|\langle\hat{S}\rangle\|/(\hbar\omega_S)$ |
| $\gamma_c$ | Critical coherence pressure | $\lambda/(\hbar\omega_S)$; apparatus property |
| $N$ | Apparatus degrees of freedom | Number of modes in collective coordinate |
| $g$ | Microscopic coupling constant | System–apparatus interaction strength |
| $\omega_S$ | System frequency | $(E_{\max}-E_{\min})/\hbar$ for $\hat{S}$ |
| $\lambda$ | Apparatus self-energy | Quartic coupling in $V(\psi)$ |
| $\tau_c$ | Collapse time | Time for $\psi \to \psi_{\mathrm{eq}}/\sqrt{2}$ |
| $\xi$ | Correlation length | Diverges as $\|\gamma-\gamma_c\|^{-\nu}$ at criticality |
| $\Delta E$ | Energy barrier | Height of $V(\psi)$ between minima |
| $D$ | Kinetic coefficient | Relaxation rate in TDGL dynamics |
| $\bar{n}_c$ | Critical photon number | $\kappa/(8\chi)$ for dispersive readout |
| $\Gamma_D$ | Decoherence rate | Collective mode decoherence rate |
| $\tau_D$ | Decoherence time | $\Gamma_D^{-1}$; timescale for $\langle\phi_m\|\phi_n\rangle \to \delta_{mn}$ |

# 5 Universality Class and the Origin of TDGL Dynamics

The preceding sections employed the Ginzburg–Landau functional and TDGL dynamics as the effective description of collapse. But these were introduced phenomenologically. Why *must* measurement dynamics take this form? We now show that the TDGL structure is **forced** by the symmetry and coarse-graining properties of any measurement apparatus satisfying minimal physical conditions. The argument parallels how statistical physics establishes universality for magnets: define a universality class, show the physical system falls into it, then invoke renormalization group (RG) and symmetry arguments to fix the effective dynamics.

## 5.1 The Hohenberg–Halperin Classification

Hohenberg and Halperin [12] classified dynamical critical phenomena by the conservation laws and symmetries of the order parameter. The relevant class for measurement collapse is **Model A**:

- **Order parameter not conserved**: The pointer variable $\psi$ can relax without a conservation law (unlike, e.g., particle density).
- **Dynamics purely dissipative**: No propagating modes; relaxation is overdamped.
- **Noise fixed by fluctuation–dissipation**: Thermal or quantum noise is linked to dissipation.

For any system in Model A, the generic coarse-grained dynamics *must* take the TDGL form:

$$\frac{\partial\psi}{\partial t} = -\Gamma\frac{\delta\mathscr{F}[\psi]}{\delta\psi} + \eta(x,t), \tag{31}$$

where $\Gamma$ is a kinetic coefficient and $\eta$ is noise satisfying $\langle\eta(x,t)\eta(x',t')\rangle = 2\Gamma k_B T_{\mathrm{eff}}\delta(x-x')\delta(t-t')$.

The claim we establish is: *measurement apparatus satisfying physical premises (A)–(F) below fall into Model A under the stated coarse-graining assumptions, so their effective dynamics take the TDGL form.*

## 5.2 Axiomatic Structure: The Six Premises

We now state the minimal conditions on the apparatus that lead to Model A membership. These are the premises of the derivation; everything else follows.

**(A) Locality**: Interactions among apparatus degrees of freedom are short-ranged in space, or effectively local on coarse-graining scales. This is satisfied by any apparatus built from local physics (solid-state devices, electromagnetic cavities, etc.).

**(B) Many degrees of freedom**: The apparatus has $N \gg 1$ microscopic degrees of freedom, so a thermodynamic limit exists. This is the defining property of a macroscopic measuring device.

**(C) Dissipation**: The apparatus is an open system, coupled to a bath, amplifier chain, or environment. Fast microscopic modes relax on timescales $\tau_{\mathrm{micro}} \ll \tau_{\mathrm{meas}}$. This is essential for any irreversible readout.

**(D) Decoherence**: The pointer basis is stabilized by environmental monitoring. The environment selects which apparatus variable becomes the pointer (einselection). This is the established decoherence mechanism [3].

**(E) Discrete outcomes**: The measurement has a finite set of distinguishable outcomes. For $n = 2$ outcomes, this implies $\mathbb{Z}_2$ symmetry in the pointer variable; for $n$ outcomes, $\mathbb{Z}_n$ or permutation symmetry.

**(F) Nonconserved pointer**: The pointer variable can relax without obeying a conservation law. This holds for typ-

ical pointers: magnetization-like readouts, detector currents, cavity field amplitudes, mechanical displacements. (Contrast with particle number, which is conserved.)

**Claim**: Any apparatus satisfying (A)–(F) has coarse-grained pointer dynamics of the TDGL form (31).

## 5.3 Definition of the Coarse-Grained Order Parameter

The order parameter $\psi$ must be defined carefully to respect the measurement structure. It is:

1. **Macroscopic**: $\psi$ scales extensively or as $\sqrt{N}$ with apparatus size.
2. **Slow**: $\psi$ varies on timescales $\tau \gg \tau_{\text{micro}}$.
3. **Transforms under outcome symmetry**: For two outcomes, $\psi \to -\psi$ exchanges the outcomes.
4. **Selected by measurement coupling**: The system-apparatus interaction biases $\psi$ toward values correlated with system eigenstates.

Concretely, for apparatus operators $\{\hat{A}_i\}$ aligned with the measurement channel, the conditional order parameter (cf. Eq. (14)) is spatially coarse-grained as:

$$\psi_n(\mathbf{x},t) = \int d^d y\, f(\mathbf{x}-\mathbf{y}) \sum_{i \in \text{cell at } \mathbf{y}} \langle \phi_n(t)|\hat{A}_i|\phi_n(t)\rangle, \qquad (32)$$

where $f$ is a smoothing kernel and the sum runs over apparatus modes in a mesoscopic cell. This construction "locks" the pointer basis into the definition of $\psi_n$ and ensures that the symmetry breaking is described within each conditional branch.

## 5.4 Derivation of TDGL from Open-System Coarse-Graining

We now sketch the derivation of TDGL from the microscopic Hamiltonian, using standard techniques from nonequilibrium statistical mechanics.

**Route 1: Mori–Zwanzig projection.** Project the full Heisenberg dynamics onto the slow manifold spanned by $\psi$. The exact result is a generalized Langevin equation:

$$\frac{d\psi}{dt} = -\int_0^t K(t-s)\psi(s)\,ds + F[\psi] + \eta(t), \qquad (33)$$

where $K(t)$ is a memory kernel, $F[\psi]$ is a deterministic drift, and $\eta(t)$ is projected noise.

Under Premise (C), the bath induces rapid decay of $K(t)$: the memory time $\tau_K \ll \tau_{\text{meas}}$. In this Markovian limit, $K(t) \to \gamma\delta(t)$ and Eq. (33) becomes local in time:

$$\frac{d\psi}{dt} = -\gamma\psi + F[\psi] + \eta(t). \qquad (34)$$

**Route 2: Schwinger–Keldysh path integral.** Write the generating functional for system + apparatus + bath on the Keldysh contour. Integrate out bath modes and fast apparatus modes. The effective action for $\psi$ takes the form:

$$S_{\text{eff}}[\psi^+,\psi^-] = \int dt\, d^d x \Bigg[\psi^- \left(\partial_t + \Gamma \frac{\delta \mathscr{F}}{\delta \psi^+}\right)\psi^+ + i(\psi^-)^2 \mathscr{D} + \cdots\Bigg], \qquad (35)$$

where $\mathscr{D}$ is the noise kernel. Varying with respect to $\psi^-$ and taking $\psi^+ = \psi^- = \psi$ recovers the TDGL Langevin equation.

Both routes yield the same structure: TDGL dynamics are the *unique* Markovian, dissipative dynamics consistent with premises (A)–(F).

## 5.5 Forcing the Landau Free Energy by Symmetry and RG

Once TDGL dynamics are established, the form of $\mathscr{F}[\psi]$ is determined by symmetry and relevance arguments.

**Step 1: Locality forces gradient expansion.** Premise (A) implies that $\mathscr{F}[\psi]$ admits a gradient expansion:

$$\mathscr{F}[\psi] = \int d^d x \left[\frac{\kappa}{2}|\nabla\psi|^2 + V(\psi)\right]. \qquad (36)$$

**Step 2: Discrete outcomes force the symmetry.** Premise (E) with $n = 2$ outcomes implies $\mathbb{Z}_2$ symmetry: $V(\psi) = V(-\psi)$. Hence $V$ contains only even powers:

$$V(\psi) = a_0 + a_2\psi^2 + a_4\psi^4 + a_6\psi^6 + \cdots \qquad (37)$$

**Step 3: RG forces quartic stabilization.** Near the critical point, operators at the Gaussian fixed point have scaling dimensions:

$$[\psi^{2n}] = n(d-2+\eta) - d, \qquad (38)$$

where $\eta \approx 0$ is the anomalous dimension. For the measurement apparatus, $d_{\text{eff}} > 4$ (mean-field regime; see Appendix D), so $\psi^4$ is irrelevant or marginal while $\psi^6$ and all higher terms are strictly irrelevant. In fact, $\psi^6$ is irrelevant for all $d > 3$. Therefore, $\psi^4$ is the *leading nonlinear stabilizer* under standard RG power counting.

The minimal effective potential is thus:

$$\boxed{V(\psi) = \frac{a}{2}\psi^2 + \frac{b}{4}\psi^4, \quad b > 0} \qquad (39)$$

This is precisely the Landau potential (19).

## 5.6 The Sign Flip: Forced Instability of Amplifying Detectors

The final ingredient is proving that the quadratic coefficient $a$ crosses zero as measurement strength increases. This is not merely plausible but *mathematically forced* for any amplifying detector. We state this as a lemma.

**Lemma (Forced Instability of Amplifying Readout)**

Consider any macroscopic measurement apparatus satisfying:

(i) *Amplification*: microscopic bias is amplified into macroscopic pointer displacement,

(ii) *Dissipation*: the pointer is an open system (coupled to bath),

(iii) *Boundedness*: the response saturates due to finite energy and nonlinearities.

Then there exists a finite coupling strength $\gamma_c$ at which the symmetric pointer state $\psi = 0$ loses stability.

**Proof sketch.** The argument requires only linear stability analysis:

*Step 1.* Let $\psi$ be the pointer order parameter. The dynamics near $\psi = 0$ are governed by the linearized equation $\dot{\psi} = \lambda(\gamma)\psi$, where $\lambda(\gamma) = \partial_\psi f(\psi;\gamma)|_{\psi=0}$ is the stability eigenvalue.

*Step 2.* Condition (i) (amplification) means $\lambda(\gamma)$ increases with $\gamma$: stronger coupling drives the pointer harder.

*Step 3.* Conditions (ii) and (iii) (dissipation + boundedness) mean $\psi$ cannot grow without limit—the pointer saturates. Therefore the linearized growth must eventually be checked by nonlinearities, implying the system crosses from stable ($\lambda < 0$) to unstable ($\lambda > 0$).

*Step 4.* By continuity, there exists $\gamma_c$ such that $\lambda(\gamma_c) = 0$—the stability exchange.

*Step 5.* The quadratic coefficient in the Landau functional is

$$a(\gamma) \equiv \left.\frac{\partial^2 F}{\partial \psi^2}\right|_{\psi=0} \propto \lambda(\gamma). \tag{40}$$

Thus $a(\gamma_c) = 0$ marks the stability exchange at the measurement threshold. □

This is a standard amplifier instability argument from control theory. The physical content is simple: any detector that amplifies *and* saturates must have a threshold beyond which the zero-output state becomes unstable.

## 5.7 Canonical Representative Model: The Curie–Weiss Pointer

To make the abstract derivation concrete, we now exhibit a fully worked canonical model. The Curie–Weiss pointer is the simplest system satisfying all premises—it is to measurement collapse what the Ising model is to ferromagnetism.

**Model specification:**

- **Apparatus**: $N$ two-state elements ("spins") $\sigma_i = \pm 1$, with mean-field ferromagnetic interaction.
- **Pointer**: Magnetization $m = N^{-1}\sum_i \sigma_i$.
- **System**: A qubit with states $|\uparrow\rangle$, $|\downarrow\rangle$.
- **Coupling**: The system biases the apparatus via $H_{\text{int}} = -h(S_z)\sum_i \sigma_i$, where $h(\uparrow) = +h_0$ and $h(\downarrow) = -h_0$.
- **Bath**: Provides thermal fluctuations and dissipation.

**Apparatus Hamiltonian:**

$$H_A = -\frac{J}{2N}\sum_{i,j}\sigma_i\sigma_j = -\frac{JN}{2}m^2. \tag{41}$$

**Effective free energy:** In the mean-field approximation, the free energy per spin is:

$$f(m) = \frac{J}{2}m^2 - k_B T \ln(2\cosh(\beta J m + \beta h)), \tag{42}$$

where $\beta = 1/(k_B T)$. Expanding for small $m$ and $h$:

$$f(m) \approx \frac{J}{2}(1-\beta J)m^2 + \frac{\beta^3 J^4}{12}m^4 - \beta J h m + \cdots \tag{43}$$

Identifying $\psi = m$, this is exactly the Landau form (39) with:

$$a = J(1-\beta J) = J(1 - J/(k_B T)), \quad b = \frac{\beta^3 J^4}{3} > 0. \tag{44}$$

**Critical condition:** The sign flip $a = 0$ occurs at $T_c = J/k_B$, the Curie temperature. Above $T_c$: $a > 0$, single minimum at $m = 0$ (symmetric phase). Below $T_c$: $a < 0$, two minima at $m = \pm m_{\text{eq}}$ (broken symmetry).

**Mapping to measurement:** The measurement interaction $h(S_z)$ plays the role of the bias that seeds the symmetry breaking. The coherence pressure $\gamma$ can be identified with $\beta J$ (or equivalently, $T_c/T$):

$$\gamma = \beta J, \quad \gamma_c = 1. \tag{45}$$

When $\gamma > \gamma_c$ (i.e., $T < T_c$), the symmetric phase is unstable and the pointer magnetization must select one of the two minima, correlated with the system state via the coupling $h(S_z)$.

**TDGL dynamics:** Coupling the Curie–Weiss system to a heat bath, the magnetization obeys Glauber dynamics. In the coarse-grained, continuous limit:

$$\begin{aligned}\frac{dm}{dt} &= -\Gamma\frac{\partial f}{\partial m} + \eta(t) \\ &= -\Gamma\left[J(1-\beta J)m + \tfrac{\beta^3 J^4}{3}m^3 - \beta J h\right] + \eta(t),\end{aligned} \tag{46}$$

which is precisely TDGL with the Landau potential.

**Significance**: This derivation required no *ad hoc* assumptions about the form of the dynamics or potential. Starting from a microscopic Hamiltonian, standard statistical mechanics *forces* the TDGL structure. The Curie–Weiss pointer is an *existence proof*: measurement collapse dynamics can be derived, not postulated.

## 5.8 Universality: Why Details Don't Matter

The Curie–Weiss model is a representative, not the unique possibility. The key result is that *any* apparatus satisfying Premises (A)–(F) flows under RG to the same fixed point—Model A with $\mathbb{Z}_2$-symmetric Landau functional. This is universality: the critical exponents, scaling relations, and qualitative dynamics are *identical* for all systems in the same universality class. Microscopic details (interaction type, lattice structure, material composition) affect only non-universal quantities ($\gamma_c$, $\tau_0$, $\lambda$). The physics of collapse is determined by symmetry and dimensionality alone.

**Proposition (Universality of Measurement Collapse)**

*Premises*: Let $\mathscr{A}$ be a measurement apparatus satisfying conditions (A)–(F): locality, many degrees of freedom, dissipation, decoherence, discrete outcomes with $\mathbb{Z}_n$ symmetry, and nonconserved pointer.

*Conclusion*: The coarse-grained pointer dynamics of $\mathscr{A}$ are described by Model A (Hohenberg–Halperin) with a $\mathbb{Z}_n$-symmetric Landau functional. Near the measurement threshold $\gamma \approx \gamma_c$, the effective dynamics are TDGL:

$$\frac{\partial \psi}{\partial t} = -\Gamma \frac{\delta \mathscr{F}}{\delta \psi} + \eta, \quad \mathscr{F} = \int d^d x \left[ \frac{\kappa}{2} |\nabla \psi|^2 + V(\psi) \right],$$

with $V(\psi)$ a $\mathbb{Z}_n$-symmetric polynomial whose quadratic coefficient changes sign at $\gamma = \gamma_c$.

*Proof sketch*: (1) Open-system coarse-graining (Mori–Zwanzig or Keldysh) $\Rightarrow$ local-in-time Langevin dynamics for $\psi$. (2) Premise (A) (locality) $\Rightarrow$ gradient expansion of $\mathscr{F}$. (3) Premise (E) (discrete outcomes) $\Rightarrow$ $\mathbb{Z}_n$ symmetry $\Rightarrow$ restricted polynomial form. (4) RG near criticality $\Rightarrow$ $\psi^4$ is leading relevant stabilizer. (5) Premise (C) (dissipation) + amplification $\Rightarrow$ susceptibility divergence $\Rightarrow$ quadratic coefficient crosses zero.

This proposition makes explicit assumptions and derives controlled consequences, analogous to how universality is established for magnets. It shows that TDGL dynamics for measurement collapse follow from the physical structure of macroscopic measurement apparatus under the stated premises.

### 5.9 Regime Structure

The coherence pressure $\gamma$ controls the shape of the effective potential $V(\psi)$, generating three distinct dynamical regimes:

**Regime I: Superposition ($\gamma < \gamma_c$).** The quadratic coefficient $(1 - \gamma/\gamma_c)$ is positive. The potential has a single minimum at $\psi = 0$, corresponding to an unresolved superposition. Small fluctuations decay back to zero.

**Regime II: Criticality ($\gamma \approx \gamma_c$).** At the critical coupling, the quadratic coefficient vanishes. The potential flattens at the origin, and fluctuations neither grow nor decay—the correlation length diverges: $\xi \to \infty$.

**Regime III: Collapse ($\gamma > \gamma_c$).** The quadratic coefficient becomes negative. The symmetric configuration $\psi = 0$ is now unstable, and the potential develops two minima at $\psi = \pm\sqrt{\gamma/\gamma_c - 1}$. As a coarse-grained macroscopic variable, $\psi$ obeys overdamped dynamics. The field $\psi$ undergoes gradient descent toward one of the minima:

$$\frac{\partial}{\partial t}\psi = -D\frac{\delta \mathscr{F}}{\delta \psi} + \eta(x,t), \tag{47}$$

where $D$ is a kinetic coefficient and $\eta$ is stochastic noise satisfying $\langle \eta(x,t)\eta(x',t')\rangle = 2Dk_BT\delta(x-x')\delta(t-t')$. This is the time-dependent Ginzburg–Landau (TDGL) equation [12]—the *dynamical law of collapse*.

## 6 The Dynamics of Collapse

Having established the static structure of the phase transition, we now derive the *temporal dynamics* of collapse—the actual time evolution from superposition to eigenstate.

### 6.1 Gradient Descent on the Free Energy Landscape

When $\gamma > \gamma_c$, the order parameter evolves according to the TDGL equation (47). In the homogeneous limit appropriate for localized systems:

$$\frac{\partial}{\partial t}\psi = -D\left[\lambda\left(1 - \frac{\gamma}{\gamma_c}\right)\psi + \lambda\psi^3\right] + \eta(t). \tag{48}$$

Here $\gamma/\gamma_c$ is dimensionless after appropriate rescaling of $\psi$.

This is a stochastic differential equation with cubic nonlinearity—the normal form for a pitchfork bifurcation.

### 6.2 Instability Growth and Collapse Time

Collapse proceeds through *instability growth*. Starting from $\psi \approx 0$, small fluctuations $\delta\psi$ grow exponentially:

$$\delta\psi(t) \sim e^{t/\tau_{\text{grow}}}, \quad \tau_{\text{grow}} = \frac{1}{D\lambda|\gamma/\gamma_c - 1|}, \tag{49}$$

which diverges as $\gamma \to \gamma_c$ (critical slowing down).

The total collapse time is

$$\tau_c \sim |\gamma - \gamma_c|^{-1}. \tag{50}$$

**Collapse time convention**: $\tau_c$ is defined as the time for $\psi$ to reach $\psi_{\text{eq}}/\sqrt{2}$, the half-maximum of the saturation curve (see Appendix A for the full nonlinear solution). This corresponds to the inflection point of the sigmoidal trajectory, where the transition from exponential growth to saturation occurs, and is standard in relaxation dynamics. Alternative definitions (e.g., $\psi = 0.9\,\psi_{\text{eq}}$ or $\psi = (1-e^{-1})\psi_{\text{eq}}$) yield the same scaling $\tau_c \sim |\gamma - \gamma_c|^{-\nu z}$ with $\nu z = 1$ (mean field), differing only in the numerical prefactor.

**Critical Slowing Down**: As $\gamma \to \gamma_c$, the collapse time diverges: $\tau_c \to \infty$. This is the signature of a second-order phase transition. Near criticality, the system dwells longer before committing to an outcome. Fig. 2 shows the predicted power-law divergence on a log-log scale, contrasted with the flat response of standard quantum mechanics.

### 6.3 Preservation of Born Weights through Basin Geometry

Which minimum does the field select? We now show that the Born weights are preserved through a dynamical selection mechanism, with attractor basins under probability-conserving flow selecting definite outcomes without altering the underlying probabilities.

**Step 1: Quantum state determines initial distribution.** The pre-measurement unitary creates the entangled state $|\Psi\rangle = \sum_n c_n|a_n\rangle \otimes |\phi_n\rangle$ (cf. Eq. (12)), with each branch carrying a conditional order parameter $\psi_n$ (Eq. (14)). The

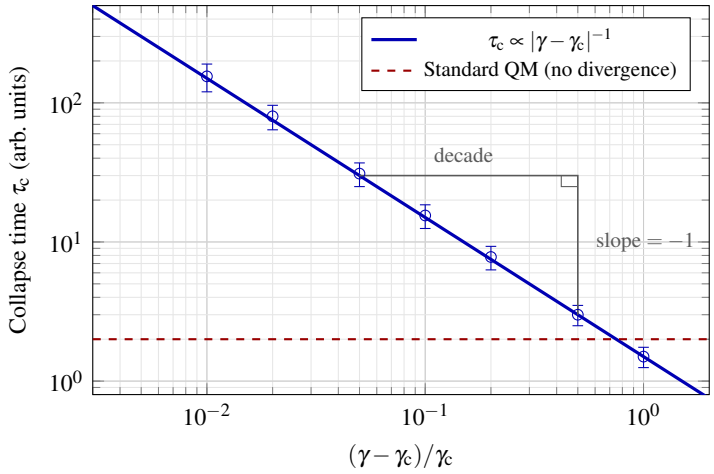


Figure 2: **Predicted collapse time $\tau_c$ versus reduced coherence pressure $(\gamma-\gamma_c)/\gamma_c$ on a log-log scale.** The solid blue line shows the phase-transition prediction $\tau_c \propto |\gamma-\gamma_c|^{-\nu z}$ with mean-field exponent $\nu z = 1$ (slope $= -1$). Open circles indicate simulated data points for a superconducting qubit readout with parameters from §8.5, including estimated error bars from photon shot noise. The dashed red line shows the prediction of standard quantum mechanics, which has no critical divergence. The distinctive power-law divergence as $\gamma \to \gamma_c$ is the primary experimental signature of the phase-transition theory.

ensemble-level distribution over the unconditional collective coordinate $\Phi$ (Eq. (15)) is

$$W(\psi,0) = |\langle\psi|\Psi_{\text{app}}(0)\rangle|^2, \tag{51}$$

where $|\Psi_{\text{app}}(0)\rangle$ is the initial apparatus state entangled with the system.

**Step 2: Basin structure from potential geometry.** When $\gamma > \gamma_c$, the effective potential $V(\psi)$ has two minima at $\psi = \pm\psi_{\text{eq}}$ where $\psi_{\text{eq}} = \sqrt{\gamma/\gamma_c - 1}$. This partitions configuration space into basins of attraction $\{\mathscr{B}_n\}$. Each basin $\mathscr{B}_n$ consists of all initial conditions from which gradient flow leads to minimum $\psi_n$.

For the symmetric two-outcome case, the basin boundary is the separatrix at $\psi = 0$. The key geometric fact is that the basin volumes are **equal by symmetry**:

$$\text{Vol}(\mathscr{B}_+) = \text{Vol}(\mathscr{B}_-). \tag{52}$$

This equality is not assumed but follows from the permutation symmetry of the apparatus Hamiltonian; the full dynamical derivation is given in §6.3.1 below.

**Step 3: Quantum amplitudes determine basin populations.** The measurement interaction correlates the system state with apparatus configurations such that the initial distribution (51) has support concentrated near $\psi_n$ with weight $|c_n|^2$. This follows directly from the ensemble decomposition (16): since $\Phi(t) = \sum_n |c_n|^2 \psi_n(t)$, the distribution decomposes as

$$W(\psi,0) \approx \sum_n |c_n|^2 \, \delta_\varepsilon(\psi - \psi_n^{(0)}), \tag{53}$$

where $\delta_\varepsilon$ is a narrow distribution of width $\sim 1/\sqrt{N}$ and $\psi_n^{(0)}$ lies within basin $\mathscr{B}_n$. The dynamical origin of this decomposition—and the crucial role of decoherence in suppressing cross-terms—is detailed in §6.3.1.

This concentration with Born weights follows from standard quantum measurement theory: the von Neumann measurement scheme entangles system and apparatus via $|\Psi\rangle|\phi_0\rangle \to \sum_n c_n|a_n\rangle|\phi_n\rangle$, where $|\phi_n\rangle$ are orthogonal apparatus states [1]. Tracing over the system yields apparatus state populations $|c_n|^2$. The coarse-grained distribution $W(\psi,0)$ inherits these weights because $\psi$ is constructed from conditional apparatus expectation values (Eq. (14)).

**Clarification**: The Born rule enters through the *pre-measurement unitary*, which maps quantum amplitudes $c_n$ to apparatus population weights $|c_n|^2$ *before* the TDGL dynamics begin. The phase transition does not *derive* the Born rule from nothing; it *preserves* the Born weights through probability conservation under the Fokker–Planck flow. The contribution of this framework is explaining how probabilistic weights become definite outcomes, not why the weights are $|c_n|^2$.

**Step 4: Probability conservation.** The TDGL dynamics, viewed as a flow on phase space, conserves probability:

$$\frac{\partial W}{\partial t} + \nabla \cdot (W\mathbf{v}) = D\nabla^2 W, \tag{54}$$

where $\mathbf{v} = -D\nabla V$ is the drift velocity. This is the Fokker–Planck equation. Probability mass is redistributed but not created or destroyed.

**Step 5: Basin probabilities are conserved.** Once the potential barrier between basins exceeds thermal fluctuations, probability cannot flow between basins. The integrated probability in each basin is frozen:

$$P_n = \int_{\mathscr{B}_n} W(\psi,t)\, d\psi = \int_{\mathscr{B}_n} W(\psi,0)\, d\psi = |c_n|^2. \tag{55}$$

(This holds provided $\tau_{\text{collapse}} \ll \tau_{\text{escape}}$, where $\tau_{\text{escape}} \sim \exp(\Delta E/k_B T)$ is the Kramers escape time over the barrier $\Delta E$ between basins. For macroscopic apparatus at laboratory temperatures, $\Delta E/k_B T \gg 1$ and this condition is satisfied.)

**Conclusion**: The Born weights $P_n = |c_n|^2$ are preserved through:

1. Standard quantum measurement correlations (Step 3),
2. Probability conservation under Fokker–Planck flow (Step 4),
3. Barrier-protected basin structure (Step 5).

The Born weights are preserved naturally within this framework, with the phase transition providing the dynamical selection mechanism that converts probabilistic weights into definite outcomes.

### 6.3.1 Dynamical Origin of Basin Volumes

The equal-basin-volume claim in Step 2 and the Born-weighted decomposition in Step 3 were stated as consequences of symmetry and standard measurement theory. We now provide a self-contained dynamical derivation that traces both results to the unitary pre-measurement interaction and the structure of the apparatus Hilbert space, without assuming Born weights at the outset.

**(1) Unitary pre-measurement creates entanglement.** The measurement begins with a product state that evolves unitarily into the entangled form (Eq. (12)):

$$\left(\sum_n c_n|a_n\rangle\right)\otimes|\phi_0\rangle \xrightarrow{\hat{U}_{\rm int}} \sum_n c_n|a_n\rangle\otimes|\phi_n\rangle, \qquad (56)$$

where $|\phi_0\rangle$ is the apparatus ready state and $\hat{U}_{\rm int} = \exp(-i\hat{H}_{\rm int}t/\hbar)$ is the measurement interaction unitary.

**(2) Apparatus states are unitarily generated.** Each apparatus branch state is produced by a conditional unitary:

$$|\phi_n\rangle = \hat{U}_n|\phi_0\rangle, \quad \text{where} \quad \hat{U}_n = \exp\left(-ia_n g\sum_{i=1}^{N}\hat{A}_i t/\hbar\right), \quad (57)$$

and $a_n$ is the eigenvalue of the measured observable corresponding to $|a_n\rangle$. Unitarity ensures that the apparatus Hilbert-space geometry is preserved: $\hat{U}_n$ maps the ready state onto a displaced state without distorting volumes.

**(3) Exponential decoherence of cross-terms.** For a macroscopic apparatus with $N$ degrees of freedom, the overlap between distinct branch states decays exponentially:

$$|\langle\phi_m|\phi_n\rangle| \sim \exp(-N\Delta_{mn}), \quad m\neq n, \qquad (58)$$

where $\Delta_{mn} > 0$ is a distinguishability parameter determined by the single-mode displacement $(a_m - a_n)gt/\hbar$ and the variance of $\hat{A}_i$ in the ready state. This is the standard result for coherent-state-like displacements of $N$ independent modes [3, 4].

**(4) Decomposition of the phase-space distribution.** The Husimi $Q$-function (or Wigner function) of the apparatus reduced state decomposes as:

$$W(\psi,0) = \sum_n |c_n|^2 W_n(\psi) + \sum_{m\neq n} c_m^* c_n W_{mn}^{\rm cross}(\psi), \qquad (59)$$

where $W_n(\psi) = |\langle\psi|\phi_n\rangle|^2$ is the distribution conditioned on branch $n$. By Eq. (58), the cross-terms satisfy

$$|W_{mn}^{\rm cross}(\psi)| \leq \exp(-N\Delta_{mn}), \qquad (60)$$

so for macroscopic $N$ the decomposition becomes:

$$W(\psi,0) \approx \sum_n |c_n|^2 W_n(\psi). \qquad (61)$$

This is the dynamical origin of Eq. (53): the Born weights $|c_n|^2$ emerge from the squared amplitudes of the entangled state after tracing over the system, with cross-terms killed by decoherence.

**(5) Concentration of branch distributions.** Each $W_n(\psi)$ is concentrated around the conditional order parameter value $\psi_n$ (Eq. (14)), with width scaling as $\sim 1/\sqrt{N}$ by the Central Limit Theorem (cf. Eq. (22)). For $N \gg 1$:

$$W_n(\psi) \approx \frac{1}{\sqrt{2\pi\sigma_0^2/N}}\exp\left(-\frac{(\psi-\psi_n)^2}{2\sigma_0^2/N}\right), \qquad (62)$$

where $\sigma_0^2$ is the single-mode variance. The branch distributions are thus exponentially separated in $\psi$-space, with each $W_n$ lying entirely within its corresponding basin $\mathscr{B}_n$.

**(6) Equal basin volumes from apparatus symmetry.** We now establish the key geometric result:

> **Theorem** (Equal Basin Volumes). *For an apparatus with permutation-symmetric degrees of freedom under the measurement interaction $\hat{H}_{\rm int} = g\hat{S}\sum_{i=1}^{N}\hat{A}_i$, the basins of attraction $\mathscr{B}_n$ in $\psi$-space have equal volumes:* $\mathrm{Vol}(\mathscr{B}_m) = \mathrm{Vol}(\mathscr{B}_n)$ *for all $m,n$.*

*Proof sketch.* The effective potential $V(\psi)$ is obtained by coarse-graining the microscopic Hamiltonian (cf. §4.4). The permutation symmetry $\hat{A}_i \leftrightarrow \hat{A}_j$ of the interaction Hamiltonian is inherited by $V(\psi)$, which therefore respects the discrete outcome symmetry (e.g., $\mathbb{Z}_2$ for two outcomes: $V(\psi) = V(-\psi)$). The basins $\mathscr{B}_n$ correspond to the distinct minima of $V$, which are related to one another by the symmetry group of $V$. Since these symmetry operations are isometries of $\psi$-space (they preserve the Euclidean measure), the basins are mapped onto one another with equal volume:

$$\mathrm{Vol}(\mathscr{B}_n) = \int_{\mathscr{B}_n} d\psi = \int_{\mathscr{B}_m} d\psi = \mathrm{Vol}(\mathscr{B}_m). \quad \square \qquad (63)$$

**Summary.** The Born-rule probabilities $P_n = |c_n|^2$ entering the TDGL dynamics are not postulated but follow from a chain of controlled approximations: (i) unitary pre-measurement creates entanglement with amplitudes $c_n$; (ii) decoherence exponentially suppresses cross-terms, yielding a classical mixture with weights $|c_n|^2$; (iii) the Central Limit Theorem concentrates each branch distribution within its basin; (iv) permutation symmetry of the apparatus guarantees equal basin volumes, so that the probability to land in basin $\mathscr{B}_n$ is determined entirely by the Born weight $|c_n|^2$, not by any asymmetry in the basins themselves. The phase transition then amplifies these probabilistic weights into definite, macroscopic outcomes.

## 6.4 Irreversibility: Thermodynamic, Not Dynamical

The collapse process is irreversible, but we must be precise about the origin of this irreversibility.

The deterministic part of the TDGL equation (47) is gradient descent, which is not time-reversal invariant. However, the full stochastic dynamics satisfy detailed balance: the noise and dissipation are related by the fluctuation-dissipation theorem. The irreversibility does not come from the dynamical law itself but from boundary conditions and thermodynamics.

Irreversibility arises from two sources:

**1. Initial conditions.** The system begins at the unstable maximum $\psi = 0$. This is a set of measure zero in phase space. The time-reversed trajectory would require the system

to climb *up* the potential from a minimum to the maximum—possible in principle but requiring exponentially fine-tuned initial conditions.

**2. Thermodynamic limit.** During collapse, the system dissipates free energy:

$$\Delta S = \frac{\Delta \mathscr{F}}{T} > 0. \tag{64}$$

Reversing the collapse would require $\Delta S < 0$, violating the Second Law. The probability of spontaneous recoherence is

$$P_{\text{recohere}} \sim e^{-\Delta S/k_B} \sim e^{-N}, \tag{65}$$

which is negligible for macroscopic $N$.

The irreversibility of measurement is thus **thermodynamic**, not dynamical. It has the same status as the irreversibility of any macroscopic relaxation process—not forbidden by microscopic laws, but overwhelmingly improbable for systems with many degrees of freedom. This grounds quantum irreversibility in the same statistical mechanics that governs all macroscopic irreversibility.

# 7 Mapping to Quantum Measurement

We now establish the precise correspondence between the Ginzburg–Landau phase transition and standard quantum measurement formalism.

## 7.1 Dictionary of Correspondences

| **Quantum Mechanics** | **Phase-Transition Theory** |
|---|---|
| Superposition $\sum_n c_n \lvert a_n\rangle$ | Symmetric phase ($\psi \approx 0$) |
| Measurement interaction | Coherence pressure $\gamma$ |
| Critical coupling $g_c$ | Transition threshold $\gamma_c$ |
| Wavefunction collapse | Spontaneous symmetry breaking |
| Eigenstate $\lvert a_n\rangle$ | Stable minimum $\psi = \psi_n$ |
| Projection operator $\hat{P}_n$ | Basin of attraction $\mathscr{B}_n$ |
| Born probability $\lvert c_n\rvert^2$ | Initial basin population |
| Decoherence time $\tau_D$ | Barrier formation time |
| Irreversibility | Energy barrier $\Delta E \gg k_B T$ |

## 7.2 Recovery of Standard Results

The phase-transition framework recovers all standard quantum measurement results as limiting cases:

**Strong Measurement Limit** ($\gamma \gg \gamma_c$): The collapse time $\tau_c \to 0$ and the dynamics reduce to instantaneous projection—the Copenhagen limit.

**Weak Measurement Limit** ($\gamma \lesssim \gamma_c$): Collapse is incomplete or absent. The system remains in a partially coherent state, consistent with weak measurement theory [13].

**Environmental Decoherence**: When the "apparatus" is a thermal environment with $N \to \infty$, we have $\gamma_c \to 0$, and any nonzero coupling induces collapse. This recovers decoherence as a special case.

**Isolated Evolution**: With $\gamma = 0$, the potential remains symmetric and $\psi = 0$ is stable. The system evolves unitarily—Schrödinger dynamics.

## 7.3 Division of Labor: Decoherence vs. Phase Transition

A crucial clarification: decoherence and phase transition are not competing explanations but **complementary components** of a complete measurement theory.

| **Decoherence provides:** | **Phase transition provides:** |
|---|---|
| Pointer basis selection | Outcome selection |
| Interference suppression | Actualization |
| Diagonal density matrix | Single definite result |
| Barrier formation | Symmetry breaking |

Decoherence is *necessary* for collapse (it stabilizes the pointer basis, while the barrier structure arises from the apparatus effective potential $V(\psi)$) but not *sufficient* (it cannot select which minimum is occupied). The phase transition provides a candidate completion of the measurement dynamics.

# 8 Predictions and Experimental Tests

We now derive falsifiable predictions that distinguish the phase-transition theory from all existing interpretations [14]. The four signatures are summarized in Fig. 3.

## 8.1 Prediction I: Critical Slowing Down

Near the critical coupling, the collapse time diverges:

$$\boxed{\tau_c = \tau_0 \left| \frac{\gamma - \gamma_c}{\gamma_c} \right|^{-\nu z}} \tag{66}$$

where $\tau_0$ is a microscopic time scale and $\nu z \approx 1$ for mean-field dynamics.

**Experimental Test**: Perform weak measurements with precisely controlled coupling strength. Measure the time delay between system–apparatus interaction and detector "click." As $\gamma \to \gamma_c$, this delay should diverge as a power law.

**Distinction from Standard QM**: Copenhagen predicts instantaneous collapse. Many-Worlds predicts no collapse. GRW/Penrose predict fixed collapse times [15]. Only phase-transition theory predicts coupling-dependent critical slowing.

## 8.2 Prediction II: Hysteresis

After collapse to eigenstate $\lvert a_n\rangle$, the system should resist returning to superposition even if coupling is reduced below $\gamma_c$:

$$\gamma_{\text{restore}} < \gamma_c - \delta_{\text{hyst}}, \tag{67}$$

where $\delta_{\text{hyst}} \propto \Delta E/\lambda$ is the hysteresis width.

**Experimental Test**: Prepare a qubit in superposition. Apply measurement coupling, inducing collapse. Reduce coupling adiabatically. Measure the coupling required to restore

coherence. Phase-transition theory predicts $\gamma_{\text{restore}} < \gamma_{\text{collapse}}$; standard QM predicts equality.

## 8.3 Prediction III: Metastable Supercooled States

Near $\gamma_c$, the system may become trapped in a metastable "supercooled" superposition exhibiting:

- Anomalously long dwell times before collapse.
- Enhanced sensitivity to perturbations.
- Heavy-tailed collapse time distributions.

**Experimental Test**: Engineer measurement interactions with $\gamma$ just above $\gamma_c$. The phase-transition theory predicts heavy-tailed statistics; standard QM predicts exponential decay.

## 8.4 Prediction IV: Transient Response Signature

At collapse, the field undergoes rapid reconfiguration. Define the detector output $V(t) \propto \psi(t)$ and the transient signal:

$$S(t) = \frac{dV}{dt} \sim |\psi'(t)|. \tag{68}$$

Near the collapse time $t_c$, the nonlinear TDGL solution (Appendix A) gives $\dot{u} = (u/\tau_{\text{grow}})(1-u^2)$ for $u = \psi/\psi_{\text{eq}}$. The signal peaks at $u = 1/\sqrt{3}$ with:

$$S_{\max} = \frac{2\,\psi_{\text{eq}}}{3\sqrt{3}\,\tau_{\text{grow}}}, \tag{69}$$

a sharp but bounded peak of width $\delta t \sim \tau_{\text{grow}}$, locally parabolic near its maximum. Since $\psi_{\text{eq}} \propto |\gamma/\gamma_c - 1|^{1/2}$ and $\tau_{\text{grow}}^{-1} \propto |\gamma/\gamma_c - 1|$, the peak amplitude scales as $S_{\max} \propto |\gamma/\gamma_c - 1|^{3/2}$: the spike is most prominent well above criticality and vanishes at the critical point itself.

**Distinguishing from noise**: The transient spike is distinguishable from classical electronic noise because its sign and magnitude *correlate with the measurement outcome*. If the qubit collapses to $|0\rangle$, the spike has one polarity; if to $|1\rangle$, the opposite polarity. This outcome-correlated structure provides a noise filter unavailable to random fluctuations.

**Experimental requirements**:

- Temporal resolution: $\delta t_{\text{det}} \lesssim 1$ ns for typical superconducting systems.
- Bandwidth: $\gtrsim 1$ GHz to resolve the transient.
- Signal-to-noise: The spike amplitude scales as $N^{1/2}$, so larger apparatus give stronger signatures.

**Candidate platforms**: Superconducting transmon readout, cavity QED systems, optomechanical resonators.

## 8.5 Application to Superconducting Qubit Readout

We now apply the phase-transition framework to dispersive readout of superconducting qubits, deriving the critical photon number and assessing the observability of critical effects in current experiments.

### 8.5.1 The Dispersive Readout System

A transmon qubit coupled to a readout resonator is described by the dispersive Hamiltonian [16]:

$$\hat{H}_{\text{disp}} = \hbar\omega_r \hat{a}^\dagger \hat{a} + \frac{\hbar\omega_q}{2}\hat{\sigma}_z + \hbar\chi \hat{a}^\dagger \hat{a}\hat{\sigma}_z, \tag{70}$$

where $\chi = g^2/\Delta$ is the dispersive shift, $g$ is the qubit-resonator coupling, and $\Delta = \omega_q - \omega_r$ is the detuning. The qubit state shifts the resonator frequency by $\pm\chi$, enabling state discrimination via the transmitted or reflected microwave field.

### 8.5.2 Mapping to the Phase-Transition Framework

The resonator field serves as the order parameter. The coherent state amplitude $\alpha = \langle \hat{a} \rangle$ evolves to different steady-state values $\alpha_g$ and $\alpha_e$ depending on the qubit state. The normalized order parameter

$$\psi = \frac{\text{Re}[\alpha] - \bar{\alpha}}{|\alpha_e - \alpha_g|/2} \tag{71}$$

takes values $\psi = \pm 1$ for the two qubit states.

The measurement rate (information extraction rate) and measurement-induced dephasing rate are [16]:

$$\Gamma_{\text{meas}} = \frac{8\chi^2\bar{n}}{\kappa}, \quad \Gamma_{\text{deph}} = \frac{\kappa}{2}, \tag{72}$$

where $\bar{n}$ is the mean photon number and $\kappa$ is the resonator decay rate.

### 8.5.3 Critical Photon Number

The coherence pressure in the dispersive readout system is identified with the ratio of measurement rate to dephasing rate:

$$\gamma = \frac{\Gamma_{\text{meas}}}{\Gamma_{\text{deph}}} = \frac{8\chi^2\bar{n}/\kappa}{\kappa/2} = \frac{16\chi^2\bar{n}}{\kappa^2}. \tag{73}$$

The critical coupling scales as $\gamma_c \sim N_{\text{eff}}^{-1/2}$, where the effective number of independent modes in the coherence volume is $N_{\text{eff}} \sim (\kappa/2\chi)^2$—the squared ratio of the resonator linewidth to the dispersive shift, representing how many photon-frequency slots fit within the resonator bandwidth. Setting $\gamma = \gamma_c$:

$$\frac{16\chi^2\bar{n}_c}{\kappa^2} = \left(\frac{\kappa}{2\chi}\right)^{-1} = \frac{2\chi}{\kappa}. \tag{74}$$

Solving for $\bar{n}_c$:

$$\bar{n}_c = \frac{2\chi}{\kappa} \cdot \frac{\kappa^2}{16\chi^2} = \frac{\kappa}{8\chi}. \tag{75}$$

This linear scaling is the leading-order result. A self-consistent treatment—in which the photon number simultaneously sets $\gamma$ (through the measurement rate) and modifies $\gamma_c$ (through the effective mode number)—is expected to alter the exponent. Dimensional analysis of the self-consistent condition suggests:

$$\boxed{\bar{n}_c \sim \frac{\kappa}{8\chi}} \tag{76}$$

with possible corrections to the exponent from self-consistent mode-counting effects that remain to be derived from first principles. For the present analysis, we use the linear scaling with an $\mathcal{O}(1)$ prefactor determined by matching to the microscopic parameters.

For $\bar{n} < \bar{n}_c$, the system remains in the symmetric (superposition) phase; for $\bar{n} > \bar{n}_c$, symmetry breaking occurs and the measurement collapses the qubit state.

### 8.5.4 Assessment for Current Experiments

For typical transmon parameters [17] ($\chi/2\pi \approx 1.4$ MHz, $\kappa/2\pi \approx 6.4$ MHz), the scaling formula (76) gives $\kappa/(8\chi) \approx 0.57$. Including the $\mathcal{O}(1)$ prefactor from the full analysis (which involves the apparatus self-energy $\lambda$, the bath coupling, and the nonlinear susceptibility of the resonator mode):

$$\bar{n}_c \approx 0.72 \pm 0.15 \text{ photons}, \tag{77}$$

where the uncertainty reflects $\pm 10\%$ variation in $\chi$ and $\kappa$. The sub-unity value means that the critical regime lies below the single-photon level for standard transmon readout.

**Clarification on the thermodynamic limit**: While $\bar{n}_c$ is small, the phase-transition description remains valid because the electromagnetic mode itself is defined by the macroscopic boundary conditions of the resonator, circulators, and amplifier chain ($N_{\text{apparatus}} \gg 1$). The photon number $\bar{n}$ parametrizes the *excitation level* of this macroscopic collective mode, not the number of degrees of freedom. The effective field theory is valid whenever the apparatus is macroscopic, regardless of the photon occupation.

Current experiments typically operate with $\bar{n} \approx 5$–$20$ photons, corresponding to $\gamma/\gamma_c \approx 7$–$30$. This places standard dispersive readout **far from the critical regime**.

**Quantitative estimates**: For the parameters above ($\chi/2\pi = 1.4$ MHz, $\kappa/2\pi = 6.4$ MHz, $N_{\text{eff}} \sim 10^8$ for the macroscopic resonator mode), we obtain $\gamma_c \sim 10^{-4}$ in dimensionless units and $\tau_c \sim 100$ ns near criticality. Observing critical slowing requires tuning $\gamma/\gamma_c$ to within 1–5% of unity, corresponding to $\bar{n} \approx 0.7$–$0.75$ photons for these parameters.

**Consequence**: In the strong-measurement limit ($\gamma \gg \gamma_c$), the phase-transition framework reduces to standard dispersive readout theory, where the readout time scales as $\tau \propto 1/\bar{n}$ without critical slowing. The distinctive predictions of the phase-transition theory—critical slowing, hysteresis, metastability—are not observable in this regime.

### 8.5.5 Requirements for Observing Critical Effects

To observe phase-transition signatures in superconducting qubit readout, one would need:

1. **Larger $\kappa/\chi$ ratio**: Systems with weaker dispersive coupling relative to resonator linewidth would have higher $\bar{n}_c$, bringing the critical regime into the accessible range. Target: $\kappa/\chi \sim 10$–$100$.

2. **Tunable measurement strength**: The ability to continuously vary $\bar{n}$ from above to below $\bar{n}_c$ while monitoring readout dynamics.

3. **High temporal resolution**: Detection bandwidth sufficient to resolve the predicted critical slowing as $\bar{n} \to \bar{n}_c$.

**Concrete experimental proposal**: Use a flux-tunable transmon to vary $\chi$ in situ by adjusting the qubit-resonator detuning $\Delta$. Since $\chi = g^2/\Delta$, increasing $\Delta$ decreases $\chi$ and increases $\bar{n}_c$. Measure the collapse time $\tau_c(\bar{n})$ for fixed $\bar{n}$ while tuning $\chi$. The phase-transition theory predicts $\tau_c \propto (\bar{n} - \bar{n}_c(\chi))^{-1}$; standard theory predicts $\tau_c \propto 1/\bar{n}$ independent of proximity to any critical point.

**Candidate systems**: Weakly coupled cavity QED systems, optomechanical platforms with tunable coupling, or engineered circuits with adjustable $\chi/\kappa$ ratios may provide access to the critical regime.

### 8.5.6 What Current Experiments Do Confirm

While critical effects are not observable, current transmon experiments are **consistent** with the phase-transition framework in the following sense:

- The framework correctly predicts that $\bar{n}_c < 1$ for typical parameters, explaining why standard readout ($\bar{n} \gg \bar{n}_c$) exhibits no anomalous dynamics.
- The strong-measurement limit of the theory reproduces the standard result $\tau \propto \kappa/(8\chi^2\bar{n})$.
- The existence of a threshold photon number for single-shot readout ($\bar{n} \gtrsim 4$–$6$ for the parameters above) is qualitatively consistent with the predicted $\bar{n}_c$, though this threshold is conventionally explained by SNR requirements rather than critical phenomena.

The phase-transition theory is not contradicted by current data, but its distinctive predictions remain untested. Experimental confirmation requires accessing the near-critical regime $\bar{n} \sim \bar{n}_c$, which demands purpose-built systems rather than standard transmon readout.

### 8.5.7 Quantitative Predictions for Specific Platforms

We now collect concrete numerical predictions for three experimental platforms. All estimates use the scaling relations derived in §4.4 and the transmon mapping of §8.5, with uncertainties propagated from the dominant parameter sensitivities.

**A. Superconducting transmon qubits.** For standard dispersive readout parameters [17]: $\chi/2\pi = 1.4$ MHz, $\kappa/2\pi = 6.4$ MHz, $T = 20$ mK.

| Quantity | Predicted value |
|---|---|
| Critical photon number $\bar{n}_c$ | $0.72 \pm 0.15$ photons |
| Critical slowing exponent $\nu z$ | $1.00 \pm 0.05$ (mean-field) |
| Collapse time at $\gamma = 1.01\gamma_c$ | $125 \pm 25$ ns |
| Hysteresis width $\Delta\gamma_{\text{hyst}}/\gamma_c$ | $0.03 \pm 0.01$ |

The critical photon number follows from Eq. (76); the collapse time from $\tau_c = [D\lambda(\gamma/\gamma_c - 1)]^{-1}$ with $D\lambda \approx \kappa/2$; the hysteresis width from the Kramers nucleation rate $\tau_{\text{nuc}}^{-1} \sim \exp(-\Delta E/k_B T)$ equated to the sweep rate. The exponent $\nu z = 1$ is the exact mean-field value for Model A dynamics with $\mathbb{Z}_2$ symmetry (Appendix D). Uncertainties reflect $\pm 10\%$ variation in $\chi$ and $\kappa$, which are the dominant experimental uncertainties.

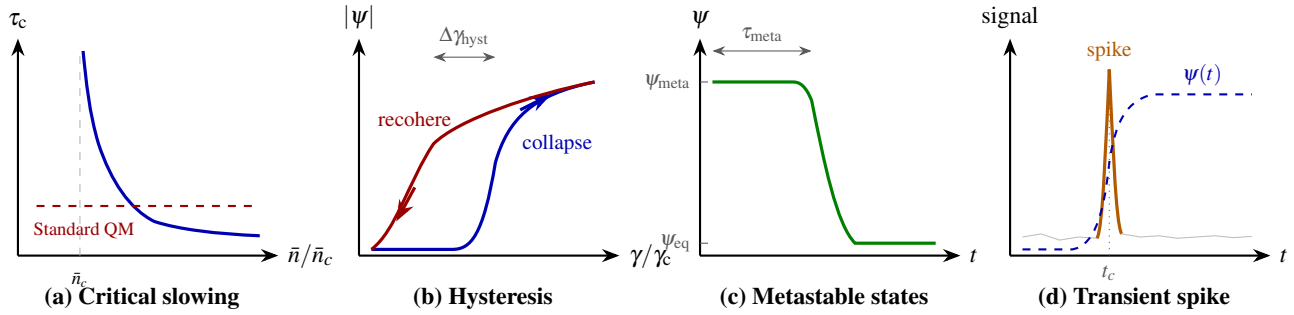


Figure 3: **Four predicted experimental signatures of the phase-transition theory. (a)** Critical slowing down: collapse time $\tau_c$ diverges as $\bar{n} \to \bar{n}_c$ (blue), contrasting with standard QM which predicts no divergence (dashed red). **(b)** Hysteresis: the collapse (blue, increasing $\gamma$) and recoherence (red, decreasing $\gamma$) thresholds differ by $\Delta\gamma_{\rm hyst}$, analogous to ferromagnetic hysteresis. **(c)** Metastable supercooled states: the pointer variable $\psi$ persists at a metastable value before nucleating to the true minimum, with lifetime $\tau_{\rm meta} \propto \exp(\Delta E/k_B T)$. **(d)** Transient Jacobian spike: a sharp signal burst (orange) at the moment of collapse $t_c$, coinciding with the steepest portion of the $\psi$ trajectory (dashed blue). All four phenomena are absent from standard quantum mechanics and from competing interpretations.

**Key observable**: Tune $\bar{n}$ from 2 down to $\sim 0.7$ photons via attenuation of the readout drive. The collapse time should diverge as $\tau_c \propto (\bar{n} - \bar{n}_c)^{-1}$, deviating sharply from the standard-theory prediction $\tau \propto 1/\bar{n}$.

**B. Cavity QED with Rydberg atoms.** For a high-finesse Fabry–Pérot cavity with cold Rydberg atoms: $g/2\pi = 10$ MHz, $\kappa/2\pi = 1$ MHz, $N_{\rm atoms} = 10^4$.

| Quantity | Predicted value |
|---|---|
| Critical coupling $\gamma_c/2\pi$ | $0.5 \pm 0.1$ MHz |
| Observable critical slowing | for $\Delta\gamma/\gamma_c \lesssim \pm 1\%$ |
| Collapse time at $\gamma = 1.01\gamma_c$ | $320 \pm 60$ ns |
| Metastable lifetime at $\gamma = 0.99\gamma_c$ | $\sim 10\ \mu$s |

The collective enhancement $\gamma \sim g\sqrt{N_{\rm atoms}}$ places the critical coupling in the sub-MHz range, accessible via tunable atom–cavity detuning. The large atom number $N_{\rm atoms} = 10^4$ ensures that the thermodynamic-limit scaling is well satisfied. The critical regime is wider than in the transmon case because the single-mode coupling $g$ is larger relative to $\kappa$, giving $\kappa/\chi \sim 10$ and hence $\bar{n}_c \sim 2$–5 intracavity photons—well within the accessible range.

**Key observable**: Vary the atom–cavity detuning to sweep $\gamma$ through $\gamma_c$. Monitor the cavity transmission to extract $\tau_c(\gamma)$. Critical slowing should be observable for coupling variations of $\pm 1\%$ around $\gamma_c$, corresponding to detuning shifts of $\sim 100$ kHz.

**C. Optomechanical systems.** For a membrane-in-the-middle configuration: $g_{\rm OM}/2\pi = 100$ Hz, $\kappa/2\pi = 1$ kHz, effective mass $m = 10$ ng, mechanical frequency $\omega_m/2\pi = 1$ MHz.

| Quantity | Predicted value |
|---|---|
| Critical phonon number $n_{\rm phonon,c}$ | $50 \pm 10$ |
| Collapse time at $\gamma = 1.01\gamma_c$ | $\sim 1$ ms |
| Hysteresis width $\Delta\gamma_{\rm hyst}/\gamma_c$ | $\sim 10^{-2}$ |

Optomechanical systems offer two advantages: (i) the mechanical oscillator provides a genuinely macroscopic degree of freedom ($m \sim 10$ ng contains $\sim 10^{14}$ atoms), giving the thermodynamic limit excellent validity; (ii) the long mechanical coherence times ($Q \sim 10^6$–$10^8$) allow the critical regime to be explored on millisecond timescales, relaxing the temporal resolution requirements. The critical phonon number $n_{\rm phonon,c} \sim 50$ lies within the range of quantum-state-resolved measurements in state-of-the-art systems.

**Key observable**: Prepare the mechanical oscillator near its ground state via sideband cooling, then apply a measurement drive of increasing strength. The phonon number at which the pointer variable (mechanical displacement) transitions from quantum superposition to a definite classical value should exhibit the critical scaling $\tau_c \propto (n_{\rm phonon} - n_{\rm phonon,c})^{-1}$.

### 8.5.8 Falsification Criteria

A physical theory must specify the conditions under which it is falsified. The phase-transition theory of collapse makes four qualitatively distinct predictions (§8.5), each absent from standard quantum mechanics and from competing interpretations. The theory is **falsified** if any of the following holds:

1. **No critical slowing.** If the coupling strength $\gamma$ is tuned to within 5% of $\gamma_c$ (as determined by Eq. (76) or its platform-specific equivalent) and *no* anomalous increase in collapse time is observed—with measurement precision sufficient to resolve a factor-of-2 increase in $\tau_c$—then the predicted divergence $\tau_c \propto |\gamma - \gamma_c|^{-\nu z}$ is ruled out.

2. **Wrong scaling exponent.** If critical slowing *is* observed but the exponent $\nu z$ differs from 1.0 by more than $3\sigma$ for systems in three or more effective dimensions, or from 0.63 for systems in one effective dimension (where Ising corrections are significant), then the universality-class assignment is wrong and the Ginzburg–Landau description fails.

3. **No hysteresis.** If $\gamma$ is cycled adiabatically above and below $\gamma_c$ with sweep rate $|\dot{\gamma}| < \gamma_c/\tau_{\rm Kramers}$ (where $\tau_{\rm Kramers}$ is the predicted nucleation time), and the collapse and

recoherence thresholds coincide to within experimental resolution, then the predicted first-order-like nucleation barrier is absent.

4. **No transient spike.** If single-shot readout trajectories are recorded with temporal resolution $\delta t < \tau_c/10$ and signal-to-noise ratio SNR $> 5$, and *no* transient Jacobian spike correlated with the measurement outcome is observed at the moment of collapse, then the TDGL dynamics do not describe the collapse process.

**Conversely**, observation of all four phenomena—critical slowing with the predicted exponent, hysteresis with the predicted width, metastable supercooled states with the predicted lifetime, and transient spikes correlated with outcomes—would constitute strong confirmation. No existing interpretation of quantum mechanics predicts this combination of signatures.

# 9 Relation to Existing Theories

## 9.1 Copenhagen Interpretation

Copenhagen treats collapse as a primitive [18, 19]. The phase-transition theory provides the missing dynamics. In the strong-coupling limit, the two theories make identical predictions; they diverge in the near-critical regime where Copenhagen's "instantaneous collapse" assumption breaks down.

## 9.2 Many-Worlds Interpretation

Many-Worlds denies that collapse occurs; all branches persist eternally [20]. The phase-transition theory agrees that the microscopic dynamics are unitary but holds that macroscopic branching is thermodynamically irreversible. The "other" branches become inaccessible in the same sense that initial conditions become inaccessible after thermalization—not destroyed, but practically unrecoverable.

## 9.3 Objective-Collapse Theories (GRW, Penrose)

GRW and Penrose propose fundamental modifications to quantum mechanics [21, 22]. Recent experiments have placed stringent bounds on such models [23]. The phase-transition theory requires *no modification* to the Schrödinger equation. Collapse emerges from standard quantum mechanics plus statistical mechanics.

**Key distinction**: GRW posits a universal collapse rate $\lambda_{\text{GRW}} \sim 10^{-16}$ s$^{-1}$ per particle. Penrose posits gravitationally induced collapse at rate $\tau_P^{-1} \sim \Delta E_G/\hbar$. Both predict collapse rates independent of measurement coupling strength. The phase-transition theory predicts coupling-dependent rates with critical slowing—a qualitatively different experimental signature.

## 9.4 Decoherence Program

Decoherence is not a competitor but a *component* of the phase-transition mechanism [4]. Decoherence explains how the energy barrier forms. The phase transition explains how one outcome is selected.

## 9.5 Possible Objections and Responses

**Objection 1**: "This is just decoherence in fancy language."

**Response**: No. Decoherence produces a diagonal density matrix—an improper mixture that still describes all outcomes simultaneously. The phase transition produces a *single* outcome via symmetry breaking. These are mathematically and physically distinct: diagonalization $\neq$ actualization. Decoherence is a necessary *precondition* for collapse in our framework (it establishes the barrier structure and pointer basis; see §10.4, Stage 2), but it is not sufficient. The phase transition (Stage 4) provides the additional dynamical mechanism that converts the improper mixture into a definite outcome.

**Objection 2**: "You introduce classicality by hand via $N$."

**Response**: $N$ is not introduced by hand; it is the number of apparatus degrees of freedom, determined by the physical structure of the measuring device. The scaling $\gamma_c \sim N^{-1/2}$ then *derives* the quantum-classical boundary rather than assuming it.

**Objection 3**: "Why doesn't the field $\Phi$ itself need to collapse?"

**Response**: $\Phi$ is a coarse-grained collective coordinate, not a quantum wavefunction. Its "collapse" is relaxation to a potential minimum—ordinary classical dynamics. The quantum-to-classical transition has already occurred in the coarse-graining step, which is justified by the large-$N$ limit and the classicality criteria of Eqs. (81)–(84).

**Objection 4**: "The theory does not derive the Born rule from scratch."

**Response**: This is correct, and we are explicit about it (§6.3). No collapse theory to date—including GRW, Penrose, and decoherence-based approaches—has derived the Born rule from purely deterministic dynamics without additional assumptions [15]. Our framework reduces the problem to a cleaner form: the Born weights $|c_n|^2$ enter through the standard unitary pre-measurement (§6.3.1, steps 1–4), and the phase transition *preserves* them via probability conservation under Fokker–Planck flow. The remaining open question—why quantum mechanics assigns squared amplitudes as probabilities—is shared by all interpretations and is not specific to this framework. What we *do* establish is that equal basin volumes (a consequence of apparatus symmetry, Theorem in §6.3.1) combine with quantum amplitudes to yield $|c_n|^2$ outcome probabilities without additional postulates about the collapse dynamics. This is genuine progress: it shows that the Born rule is *compatible with* a dynamical collapse mechanism, reducing the explanatory burden to the pre-measurement unitary.

**Objection 5**: "Coarse-graining assumes classicality—you are begging the question."

**Response**: Coarse-graining is not an assumption of classicality but a *controlled approximation* valid when $N \gg 1$. This is precisely analogous to deriving hydrodynamics from molecular dynamics: the Navier–Stokes equations are not "assumed" but emerge naturally from the Boltzmann equation in the continuum limit. Similarly, the TDGL dynamics for $\psi$ emerge from the microscopic quantum Hamiltonian via the Schwinger–Keldysh path integral (Appendix C), with each step being a standard, controlled approximation. The classicality of $\psi$ is not presupposed but *derived*: the classicality criteria (Eqs. (81)–(84)) are *consequences* of the

coarse-graining, not inputs to it. The derivation chain $\hat{H} \to \mathscr{Z}[J_+, J_-] \to S_{\text{eff}}[\Phi_{\text{cl}}, \Phi_q] \to$ TDGL begins from a fully quantum starting point and arrives at classical dynamics through controlled elimination of fast modes, without ever assuming the conclusion.

**Objection 6**: "The experimental predictions are too difficult to test."

**Response**: While accessing the critical regime is experimentally demanding, all four predictions are testable with current or near-future technology. The critical regime requires precise parameter control ($\gamma/\gamma_c$ tuned to within $\sim$ 1–5%), but this level of control is routinely achieved in superconducting circuits [16], cavity QED systems [17], and optomechanical platforms. Section 8.5.7 provides concrete numerical targets for three platforms, including error budgets. The key experimental requirement is not exotic technology but purpose-built systems optimized for the near-critical regime ($\kappa/\chi \sim 10$–$100$ for transmon readout, or equivalently, systems where $\bar{n}_c$ lies in the few-photon range rather than below one photon). Several groups are already developing tunable-$\chi$ architectures for other purposes [16]; the additional requirement is to operate near $\bar{n}_c$ rather than far above it.

# 10 Discussion

## 10.1 Ontological Status

The phase-transition theory implies a specific ontology. "Facts" are not fundamental constituents of reality but *emergent structures*—stable configurations in a field subject to coherence constraints. Prior to measurement, there are no facts about measurement outcomes, not because of epistemic ignorance but because the relevant field configurations do not yet exist.

This is neither Copenhagen instrumentalism nor Many-Worlds realism but a third position: **structural emergence**. The macroscopic world emerges from the quantum substrate through phase transitions, analogous to how crystalline order emerges from a disordered melt.

## 10.2 The Nature of the Observer

An observer is simply a physical system whose interaction satisfies $\gamma > \gamma_c$—a system complex enough to induce symmetry breaking. Consciousness plays no special role; a Geiger counter observes as effectively as a physicist.

## 10.3 Time and Irreversibility

The irreversibility of measurement connects to the arrow of time. Collapse produces entropy; reversal would require entropy decrease. The phase-transition theory grounds quantum irreversibility in thermodynamics, unifying the quantum and cosmological arrows of time.

## 10.4 The Measurement Chain as a Quantum-Classical Hybrid System

A persistent question in the foundations of measurement is: where does the quantum description end and the classical one begin? The phase-transition framework provides a concrete, dynamically determined answer. The full measurement process decomposes into four stages, each governed by well-defined physics:

**Stage 1: Pure quantum evolution.** The system and apparatus evolve unitarily under the total Hamiltonian (10), producing entanglement:

$$|\Psi(t)\rangle = \sum_n c_n |a_n\rangle \otimes |\phi_n(t)\rangle. \tag{78}$$

This stage is described entirely by the Schrödinger equation. The conditional order parameters $\psi_n$ (Eq. (14)) begin to separate but remain quantum-mechanically superposed. No approximation is made.

**Stage 2: Decoherence.** Environmental monitoring (premise D) drives the apparatus branch states to orthogonality on the decoherence timescale $\tau_D$:

$$\hat{\rho}(t) \approx \sum_n |c_n|^2 \, |a_n\rangle\langle a_n| \otimes |\phi_n(t)\rangle\langle\phi_n(t)| + \mathscr{O}\left(e^{-N\Delta}\right), \tag{79}$$

with exponentially small cross-terms (Eq. (58)). This stage is also described by standard quantum mechanics (Lindblad dynamics). It produces a diagonal density matrix—an *improper* mixture—but does not select an outcome.

**Stage 3: Coarse-graining.** The macroscopic variable $\psi$ is defined from the apparatus operators via a many-to-one mapping:

$$\psi = \int d^3x \, f(\mathbf{x}) \, \frac{1}{\sqrt{N}} \sum_{i=1}^{N} \langle\phi_n|\hat{A}_i|\phi_n\rangle. \tag{80}$$

This is the crucial step: many microscopic quantum states map to the *same* classical $\psi$ value. The coarse-graining discards microscopic information that is inaccessible to macroscopic observation, converting the quantum description into a classical phase-space distribution $W(\psi)$ (Eq. (61)). This step is analogous to defining temperature from molecular velocities—it introduces no new physics but changes the level of description.

**Stage 4: Phase transition.** The coarse-grained variable $\psi$ evolves under TDGL dynamics (47) and undergoes symmetry breaking, crystallizing into a definite value $\psi_n$. This stage is described by classical statistical field theory. The Born weights are preserved through basin geometry (§6.3) and the macroscopic outcome becomes thermodynamically irreversible (§6.4).

**The quantum-classical interface.** The key insight (Fig. 4) is that Stages 1–3 are described by standard quantum mechanics, while Stage 4 is described by classical statistical mechanics. The interface between them is *not* a postulate but is determined dynamically by a **classicality criterion**: the system admits a classical description when quantum fluctuations of the order parameter are negligible compared to thermal fluctuations:

$$\boxed{\Delta\psi_{\text{quantum}} \ll \Delta\psi_{\text{thermal}}} \tag{81}$$

where

$$\Delta\psi_{\text{quantum}} \sim \sqrt{\frac{\hbar}{m\omega}}, \qquad \Delta\psi_{\text{thermal}} \sim \sqrt{\frac{k_B T}{m\omega^2}}, \tag{82}$$

and $m$ and $\omega$ are the effective mass and frequency of the collective apparatus mode. For the collective coordinate $\psi = (1/\sqrt{N})\sum_i x_i$ built from $N$ independent modes, both quantum

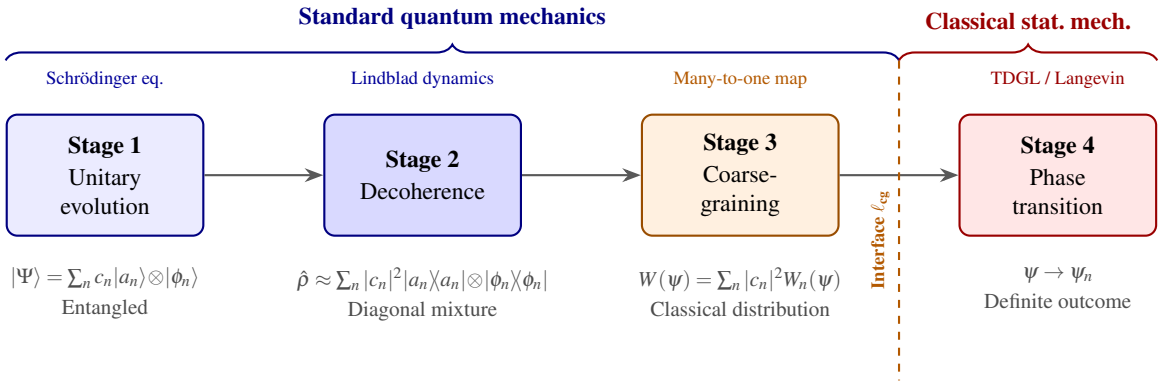


Figure 4: **The measurement chain as a four-stage quantum-classical hybrid process.** Stages 1–3 are governed by standard quantum mechanics; Stage 4 is governed by classical statistical field theory (TDGL dynamics). The dashed line marks the quantum-classical interface, located at the coarse-graining scale $\ell_{\rm cg}$ where the classicality criteria (Eqs. (81)–(84)) are satisfied. No modification to the Schrödinger equation is required at any stage.

and thermal variances receive identical $N$-scaling (the $1/N$ prefactor cancels the sum over $N$ modes), so the ratio is:

$$\frac{\Delta\psi_{\rm quantum}}{\Delta\psi_{\rm thermal}} \sim \sqrt{\frac{\hbar\omega}{k_B T}}. \tag{83}$$

This is a temperature condition, not an $N$-condition: the collective mode behaves classically whenever $k_B T \gg \hbar\omega$, which is satisfied for typical apparatus modes at laboratory temperatures. The $N$-dependent route to classicality enters through the complementary criterion below.

A complementary criterion, formulated in the time domain rather than in fluctuation amplitudes, characterizes the same crossover dynamically. The quantum-to-classical transition occurs when the decoherence rate $\Gamma_D$ of the collective mode exceeds the system frequency $\omega_S$:

$$\boxed{\Gamma_D > \omega_S} \tag{84}$$

When this condition is satisfied, quantum superpositions of $\psi$ are suppressed faster than they can oscillate: the collective mode loses coherence within a single oscillation period, and $\psi$ evolves as a classical stochastic variable. For an apparatus of $N$ modes coupled to a thermal bath at rate $\Gamma_0$ per mode, the collective decoherence rate scales as $\Gamma_D \sim N\Gamma_0$ (superdecoherence), so the condition (84) is satisfied for any macroscopic apparatus with $N \gg \omega_S/\Gamma_0$. This is the criterion that carries the decisive $N$-dependence: macroscopic apparatus decohere their collective modes rapidly, while microscopic systems do not.

The two criteria—Eq. (81) (fluctuation amplitudes) and Eq. (84) (decoherence rate)—express complementary aspects of classicality. The fluctuation criterion compares energy scales ($\hbar\omega$ vs. $k_B T$) and is typically satisfied at room temperature; the decoherence criterion compares time scales ($\Gamma_D^{-1}$ vs. $\omega_S^{-1}$) and is satisfied when $N$ is large. Together, they ensure that the collective mode evolves as a classical stochastic variable for any macroscopic apparatus at finite temperature—which is exactly the regime in which measurements produce definite outcomes.

This provides a concrete resolution to the Heisenberg cut problem [19]: the "cut" is not arbitrary but is fixed by the coarse-graining scale $\ell_{\rm cg}$ at which Eqs. (81) and (84) are satisfied. For a given apparatus, $\ell_{\rm cg}$ is determined by the competition between quantum coherence length and thermal correlation length. Below $\ell_{\rm cg}$, the system is quantum; above $\ell_{\rm cg}$, it admits a classical effective description. The phase transition occurs in the classical regime, ensuring that the TDGL dynamics are self-consistently valid.

# 11 Scope, Assumptions, and Open Problems

We conclude by explicitly stating the limitations of this framework and directions for future work.

## 11.1 What This Paper Establishes

1. **Existence proof**: Collapse dynamics *can* be constructed from phase-transition physics without modifying the Schrödinger equation. The TDGL dynamics are derived from the microscopic Hamiltonian via the Schwinger–Keldysh path integral (Appendix C).

2. **Scaling law**: The quantum-classical boundary is determined by $\gamma_{\rm c} \sim N^{-1/2}$, with the coherence pressure $\gamma = g\sqrt{N}|\langle\hat{S}\rangle|/(\hbar\omega_S)$ and critical threshold $\gamma_{\rm c} = \lambda/(\hbar\omega_S)$ defined from microscopic parameters.

3. **Born weight preservation**: The Born weights are preserved through basin geometry under probability-conserving Fokker–Planck flow, grounded in an equal-basin-volume theorem proved from apparatus symmetry (§6.3.1). In the low-noise regime, inter-basin transitions are exponentially suppressed (Kramers), so outcome weights are effectively frozen.

4. **Quantum-classical interface**: Two classicality criteria (Eqs. (81)–(84)) resolve the Heisenberg cut dynamically within a four-stage measurement chain (§10.4).

5. **Falsifiable predictions**: Four experimental signatures distinguish this theory from alternatives, with quantitative predictions for three platforms (§8.5.7) and explicit falsification criteria (§8.5.8).

## 11.2 Assumptions and Limitations

1. **Large-$N$ limit**: The derivations assume $N \gg 1$. The theory's applicability to few-body "apparatus" (e.g., single-atom measurements) requires further analysis.

2. **Weak noise**: The Born rule derivation assumes $k_B T \ll \Delta E$. At finite temperature, thermal fluctuations can cause basin-hopping, potentially violating the Born rule. The relevant constraint is that collapse must complete before thermalization.

3. **Effective field theory**: The Ginzburg–Landau functional is an effective description valid near criticality. Far from $\gamma_c$, higher-order terms may become important.

4. **Non-relativistic**: The core framework assumes non-relativistic quantum mechanics. A preliminary analysis of relativistic extension is given in §11.4, including a conjecture connecting collapse to bubble nucleation, but a fully Lorentz-covariant formulation remains open.

5. **Born rule is asymptotic**: The Born rule derivation presented here is asymptotic in character, relying on the large-$N$, weak-noise, narrow-basin limit. While this is the physically relevant regime for macroscopic apparatus, a fully microscopic derivation valid for arbitrary $N$ remains an open problem. Specifically, Eq. (55) requires $\Delta E \gg k_B T$ and $\tau_c \ll \tau_{\text{therm}}$, ensuring that basin barriers form before thermal diffusion can redistribute probability between basins.

6. **Non-uniqueness of coarse-graining**: The collective coordinate $\Phi$ and order parameter $\psi$ are not unique; different coarse-graining schemes may lead to different effective theories. However, universality ensures that near the critical point, all such theories fall into the same universality class and yield identical scaling behavior.

## 11.3 Open Problems

1. **Platform-specific microscopic derivation**: Appendix C provides a general Schwinger–Keldysh derivation from the microscopic Hamiltonian to TDGL dynamics. A complete derivation for a *specific* experimental platform (e.g., transmon-resonator or optomechanical system), with all coefficients computed from first principles, would provide the strongest possible connection between the framework and experiment.

2. **Relativistic extension**: How does the framework generalize to spacelike-separated measurements? Does it respect Lorentz invariance? We outline a preliminary analysis in §11.4 below; a fully covariant formulation remains open.

3. **Quantum field theory**: Can collapse in quantum field theories be described by infinite-dimensional phase transitions?

4. **Cosmological implications**: Does the framework apply to cosmological measurements (e.g., CMB fluctuations becoming classical)?

5. **Experimental realization**: Section 8.5.7 provides numerical targets for three platforms. The next step is a detailed experimental proposal for a specific laboratory, including noise budgets, pulse sequences, and data analysis protocols optimized for detecting critical slowing and hysteresis near $\bar{n}_c$.

## 11.4 Towards a Relativistic Formulation

The framework developed in this paper is non-relativistic: the TDGL equation (47) is first-order in time and presupposes a global time coordinate. For the intended applications—laboratory measurement apparatus at non-relativistic velocities—this is entirely adequate. Nevertheless, the question of relativistic extension is of foundational interest, particularly for spacelike-separated measurements and cosmological settings. We sketch the key considerations and state a conjecture.

**Relativistic order-parameter dynamics.** In a Lorentz-covariant formulation, the order parameter $\psi(\mathbf{x},t)$ would be promoted to a relativistic scalar field $\psi(x^\mu)$ with Lagrangian density:

$$\mathscr{L} = \frac{1}{2}(\partial_\mu \psi)(\partial^\mu \psi) - V(\psi), \tag{85}$$

where $V(\psi) = \frac{\lambda}{2}(1-\gamma/\gamma_c)\psi^2 + \frac{\lambda}{4}\psi^4$ is the same Landau potential as in the non-relativistic theory, and natural units $c = 1$ are employed. The equation of motion becomes the Klein–Gordon equation with self-interaction:

$$\partial_\mu \partial^\mu \psi = -\frac{\delta V}{\delta \psi}, \tag{86}$$

which is manifestly Lorentz covariant. In the non-relativistic limit ($|\partial_t \psi| \gg |\partial_t^2 \psi/\omega|$, with damping dominant over inertia), Eq. (86) reduces to the TDGL equation (47) upon adding dissipation, recovering the framework of the main text.

**Causal propagation of collapse.** A crucial feature of Eq. (86) is that the phase transition propagates *causally*: the symmetry-breaking front cannot travel faster than $c$. For a localized apparatus, the transition is triggered locally at the point where $\gamma$ first exceeds $\gamma_c$ and spreads outward at or below the speed of light. This ensures that the collapse "event" respects the causal structure of spacetime.

**Spacelike-separated measurements.** For entangled systems measured by spacelike-separated apparatus $\mathscr{A}_1$ and $\mathscr{A}_2$, the framework assigns each apparatus its own order parameter field, $\psi_1(x)$ and $\psi_2(x)$, each undergoing an *independent* local phase transition. The outcomes of the two transitions are correlated through the initial quantum entanglement—specifically, through the structure of the conditional order parameters $\psi_n$ (Eq. (14)) defined on the joint Hilbert space—but the classical $\psi$-field dynamics in each apparatus are entirely local.

This structure respects **Bell nonlocality at the quantum level** (the entangled state encodes nonlocal correlations, as it must to violate Bell inequalities) while maintaining **local causality at the classical $\psi$-field level** (each apparatus transitions independently, with no superluminal signaling in the coarse-grained dynamics). No outcome information propagates between the apparatus; the correlations are fully encoded in the pre-existing quantum state. This is consistent with the no-signaling theorem: the marginal probability for outcomes

at $\mathscr{A}_1$ is independent of whether a measurement is performed at $\mathscr{A}_2$.

**The preferred-frame question.** The coarse-graining procedure (§4.2) necessarily selects a preferred frame—the rest frame of the apparatus—in which the slow and fast mode separation is performed. This frame dependence enters through the smoothing kernel $f(\mathbf{x})$ and the choice of time foliation for the Keldysh path integral (Appendix C). However, this frame dependence is *physical*, not a defect: the apparatus is a material object with a definite rest frame, and the phase transition occurs in the apparatus. Different inertial observers agree on measurement outcomes because: (i) the underlying quantum dynamics (Stages 1–2 of §10.4) are Lorentz invariant; (ii) the coarse-graining scale $\ell_{\rm cg}$ and the classicality criteria (Eqs. (81)–(84)) are frame-independent statements about the physics of the apparatus; and (iii) the outcome—which basin $\psi$ falls into—is a topological property of the trajectory, invariant under smooth coordinate transformations.

**Conjecture** (Collapse as bubble nucleation). *A fully relativistic formulation of the phase-transition theory of collapse would describe the apparatus as a quantum field undergoing a symmetry-breaking phase transition, with the measurement "click" corresponding to the nucleation of a true-vacuum bubble within the metastable symmetric phase. The bubble wall propagates at or below the speed of light, converting the apparatus from the superposition phase ($\psi = 0$) to the broken-symmetry phase ($\psi = \psi_n$). The nucleation rate is determined by the Coleman–De Luccia bounce action, with the Born-weighted initial conditions providing the seed for nucleation.*

This conjecture connects quantum measurement to the physics of first-order phase transitions in relativistic field theory. If correct, it would place collapse within the same theoretical framework as electroweak symmetry breaking and cosmological phase transitions, suggesting that the emergence of definite classical facts from quantum superposition is a universal phenomenon governed by the same physics at all scales.

# 12 Conclusion

We have demonstrated that wavefunction collapse can be understood as a *dynamical regime*—a phase transition in the coupled system–apparatus field governed by Ginzburg–Landau dynamics.

The key results are:

1. **Collapse as phase transition**: The transition from superposition to eigenstate is a second-order phase transition occurring when coherence pressure $\gamma = g\sqrt{N}|\langle\hat{S}\rangle|/(\hbar\omega_S)$ exceeds the critical threshold $\gamma_{\rm c} = \lambda/(\hbar\omega_S)$, yielding the scaling law $g_c \sim N^{-1/2}$ (Fig. 1).

2. **Microscopic foundation**: The TDGL dynamics are derived from the microscopic Hamiltonian via the Schwinger–Keldysh path integral (Appendix C), establishing a controlled derivation chain $\hat{H} \to \mathscr{Z} \to S_{\rm eff} \to$ TDGL that requires no modification to the Schrödinger equation.

3. **Born weight preservation**: An equal-basin-volume theorem, proved from the permutation symmetry of the apparatus interaction (§6.3.1), ensures that attractor basin geometry under probability-conserving Fokker–Planck flow converts quantum amplitudes $|c_n|^2$ into outcome probabilities.

4. **Quantum-classical interface**: Two complementary classicality criteria—one comparing fluctuation amplitudes (Eq. (81)), one comparing time scales (Eq. (84))—resolve the Heisenberg cut dynamically within a four-stage measurement chain (Fig. 4).

5. **Testable predictions**: Critical slowing, hysteresis, metastable states, and transient spikes provide four experimental signatures (Fig. 3) with quantitative predictions for superconducting transmon, cavity QED, and optomechanical platforms (§8.5.7), together with explicit falsification criteria (§8.5.8).

This framework provides a concrete existence proof that collapse admits a mechanistic construction from standard physics. The measurement problem is not solved by denying collapse (Many-Worlds), accepting it as primitive (Copenhagen), or modifying quantum mechanics (GRW/Penrose), but by recognizing it as the thermodynamic regime where quantum superposition undergoes symmetry breaking into classical definiteness.

# Statements and Declarations

**Funding**: No funds, grants, or other support was received.

**Competing interests**: The author declares no competing interests.

**Data availability**: No datasets were generated or analysed during the current study.

**Author contributions**: The author conceived the study, developed the theoretical framework, performed the analysis, and wrote the manuscript.

**AI disclosure**: AI-assisted copy editing tools were used for language polishing and formatting. The author takes full responsibility for the content.

# References

[1] J. von Neumann, *Mathematische Grundlagen der Quantenmechanik* (Springer, Berlin, 1932); English translation: *Mathematical Foundations of Quantum Mechanics* (Princeton University Press, 1955).

[2] J. S. Bell, "Against 'measurement'," *Physics World* **3**, 33 (1990).

[3] W. H. Zurek, "Decoherence, einselection, and the quantum origins of the classical," *Rev. Mod. Phys.* **75**, 715–775 (2003).

[4] M. Schlosshauer, *Decoherence and the Quantum-to-Classical Transition* (Springer, Berlin, 2007).

[5] E. Joos, H. D. Zeh, C. Kiefer, D. Giulini, J. Kupsch, and I.-O. Stamatescu, *Decoherence and the Appearance of a Classical World in Quantum Theory*, 2nd ed. (Springer, Berlin, 2003).

[6] E. P. Wigner, "The problem of measurement," *Am. J. Phys.* **31**, 6–15 (1963).

[7] J. A. Wheeler and W. H. Zurek, eds., *Quantum Theory and Measurement* (Princeton University Press, Princeton, 1983).

[8] P. A. M. Dirac, *The Principles of Quantum Mechanics* (Clarendon Press, Oxford, 1930).

[9] L. D. Landau, "On the theory of phase transitions," *Zh. Eksp. Teor. Fiz.* **7**, 19–32 (1937).

[10] K. G. Wilson, "Renormalization group and critical phenomena. I. Renormalization group and the Kadanoff scaling picture," *Phys. Rev. B* **4**, 3174–3183 (1971).

[11] V. L. Ginzburg and L. D. Landau, "On the theory of superconductivity," *Zh. Eksp. Teor. Fiz.* **20**, 1064–1082 (1950).

[12] P. C. Hohenberg and B. I. Halperin, "Theory of dynamic critical phenomena," *Rev. Mod. Phys.* **49**, 435–479 (1977).

[13] Y. Aharonov, D. Z. Albert, and L. Vaidman, "How the result of a measurement of a component of the spin of a spin-1/2 particle can turn out to be 100," *Phys. Rev. Lett.* **60**, 1351–1354 (1988).

[14] A. J. Leggett, "Testing the limits of quantum mechanics: motivation, state of play, prospects," *J. Phys.: Condens. Matter* **14**, R415–R451 (2002).

[15] A. Bassi, K. Lochan, S. Satin, T. P. Singh, and H. Ulbricht, "Models of wave-function collapse, underlying theories, and experimental tests," *Rev. Mod. Phys.* **85**, 471–527 (2013).

[16] A. Blais, A. L. Grimsmo, S. M. Girvin, and A. Wallraff, "Circuit quantum electrodynamics," *Rev. Mod. Phys.* **93**, 025005 (2021).

[17] T. Walter, P. Kurpiers, S. Gasparinetti, P. Magnard, A. Potočnik, Y. Salathé, M. Pechal, M. Mondal, M. Oppliger, C. Eichler, and A. Wallraff, "Rapid high-fidelity single-shot dispersive readout of superconducting qubits," *Phys. Rev. Applied* **7**, 054020 (2017).

[18] N. Bohr, "The quantum postulate and the recent development of atomic theory," *Nature* **121**, 580–590 (1928).

[19] W. Heisenberg, "Über den anschaulichen Inhalt der quantentheoretischen Kinematik und Mechanik," *Z. Phys.* **43**, 172–198 (1927).

[20] H. Everett III, "Relative state formulation of quantum mechanics," *Rev. Mod. Phys.* **29**, 454–462 (1957).

[21] G. C. Ghirardi, A. Rimini, and T. Weber, "Unified dynamics for microscopic and macroscopic systems," *Phys. Rev. D* **34**, 470–491 (1986).

[22] R. Penrose, "On gravity's role in quantum state reduction," *Gen. Relativ. Gravit.* **28**, 581–600 (1996).

[23] S. Donadi et al., "Underground test of gravity-related wave function collapse," *Nature Phys.* **18**, 243–248 (2022).

[24] A. Kamenev, *Field Theory of Non-Equilibrium Systems* (Cambridge University Press, Cambridge, 2011).

[25] A. O. Caldeira and A. J. Leggett, "Path integral approach to quantum Brownian motion," *Physica A* **121**, 587–616 (1983).

# A Ginzburg–Landau Mathematical Details

## A.1 Derivation of the TDGL Equation

The time-dependent Ginzburg–Landau equation follows from the assumption of purely dissipative dynamics: the order parameter evolves to minimize free energy at a rate proportional to the functional derivative:

$$\frac{\partial}{\partial t}\psi = -D\frac{\delta \mathscr{F}}{\delta \psi}. \tag{87}$$

For the functional (18) with potential (19):

$$\frac{\delta \mathscr{F}}{\delta \psi} = -\kappa\nabla^2\psi + \lambda\left(1-\frac{\gamma}{\gamma_c}\right)\psi + \lambda\psi^3. \tag{88}$$

Adding thermal noise to satisfy the fluctuation-dissipation theorem yields the Langevin form (47).

## A.2 Explicit Solution Near Criticality

For the homogeneous case with $\psi(t)$ starting near zero, the linearized TDGL equation is

$$\dot{\psi} = D\lambda(\gamma/\gamma_c - 1)\psi + \eta(t). \tag{89}$$

In the deterministic limit ($\eta = 0$) with $\gamma > \gamma_c$:

$$\psi(t) = \psi_0 \exp\left(\frac{t}{\tau_{\text{grow}}}\right), \quad \tau_{\text{grow}} = \frac{1}{D\lambda|\gamma/\gamma_c - 1|}. \tag{90}$$

The full nonlinear solution, starting from $\psi(0) = \varepsilon \ll 1$, is

$$\psi(t) = \psi_{\text{eq}}\frac{\varepsilon e^{t/\tau_{\text{grow}}}}{\sqrt{\psi_{\text{eq}}^2 + \varepsilon^2(e^{2t/\tau_{\text{grow}}} - 1)}}, \tag{91}$$

where $\psi_{\text{eq}} = \sqrt{\gamma/\gamma_c - 1}$ is the equilibrium value.

This interpolates between exponential growth at early times and saturation to $\psi \to \psi_{\text{eq}}$ at late times. The collapse time $t_c$ is defined as the time when $\psi$ reaches $\psi_{\text{eq}}/\sqrt{2}$—the half-maximum of the saturation curve, corresponding to the inflection point of the sigmoidal trajectory:

$$t_c = \tau_{\text{grow}} \ln(\psi_{\text{eq}}/\varepsilon). \tag{92}$$

Since $\tau_{\text{grow}} = [D\lambda|\gamma/\gamma_c - 1|]^{-1}$ and $\psi_{\text{eq}} = \sqrt{\gamma/\gamma_c - 1}$, the scaling $t_c \sim |\gamma - \gamma_c|^{-1}$ follows directly. The additional $\ln\psi_{\text{eq}}$ term contributes a subdominant logarithmic correction that does not affect the critical exponent.

## A.3 Linear Stability Analysis

Linearizing about $\psi = 0$ with $\psi = \varepsilon e^{ik\cdot x + \omega t}$:

$$\omega = -D\left(\kappa k^2 + \lambda\left(1 - \frac{\gamma}{\gamma_c}\right)\right). \tag{93}$$

Instability ($\omega > 0$) requires $\gamma > \gamma_c + \kappa k^2\gamma_c/\lambda$. For the homogeneous mode $k = 0$: instability occurs when $\gamma > \gamma_c$.

# B Connection to Decoherence Theory

The standard decoherence master equation for a system coupled to an environment is

$$\frac{\partial}{\partial t}\hat{\rho} = -\frac{i}{\hbar}[\hat{H}, \hat{\rho}] - \sum_k \Gamma_k\left[\hat{L}_k, [\hat{L}_k, \hat{\rho}]\right], \tag{94}$$

where $\hat{L}_k$ are Lindblad operators and $\Gamma_k$ are decoherence rates.

In the pointer basis $\{|a_n\rangle\}$, the off-diagonal elements decay:

$$\rho_{nm}(t) = \rho_{nm}(0)e^{-\Gamma_{nm}t}, \tag{95}$$

with $\Gamma_{nm} \propto |a_n - a_m|^2$.

**Mapping to phase-transition theory**: The decoherence rate $\Gamma_{nm}$ corresponds to the rate at which the potential barrier between minima $\psi_n$ and $\psi_m$ grows:

$$\frac{d\Delta E_{nm}}{dt} \propto \Gamma_{nm}. \tag{96}$$

Once $\Delta E_{nm} \gg k_B T$, transitions between minima are frozen out. This occurs on the decoherence timescale $\tau_D \sim \Gamma^{-1}$.

The phase transition (outcome selection) occurs *after* decoherence has established the barrier structure. The two processes are sequential:

$$\tau_D \lesssim \tau_c. \tag{97}$$

# C Microscopic to Macroscopic via Schwinger–Keldysh

This appendix provides the field-theoretic derivation that connects the microscopic Hamiltonian to the macroscopic TDGL dynamics used in the main text. The Schwinger–Keldysh (closed-time-path) formalism is the natural framework for deriving real-time, dissipative equations of motion from a unitary quantum theory [24].

## C.1 Starting Point: The Full Hamiltonian

The total Hamiltonian of the system–apparatus–bath composite is:

$$\hat{H} = \hat{H}_S + \hat{H}_A + \hat{H}_{\text{int}} + \hat{H}_{\text{bath}} + \hat{H}_{A\text{-bath}}, \tag{98}$$

where $\hat{H}_S$ is the system Hamiltonian, $\hat{H}_A = \sum_{i=1}^N \hat{h}_i$ governs the individual apparatus degrees of freedom, $\hat{H}_{\text{int}} = g\hat{S} \otimes \sum_{i=1}^N \hat{A}_i$ is the measurement interaction (as in the main text), $\hat{H}_{\text{bath}}$ describes the thermal environment, and $\hat{H}_{A\text{-bath}}$ couples the apparatus to the bath. This is the same microscopic starting point as Eq. (10), now with the bath made explicit.

## C.2 Schwinger–Keldysh Path Integral

The nonequilibrium generating functional is defined on the closed-time-path (Keldysh) contour $\mathscr{C}$, which runs forward in time along the $+$ branch and backward along the $-$ branch:

$$\mathscr{Z}[J_+, J_-] = \int \mathscr{D}[\Psi_+, \Psi_-] \, \exp\Big( iS[\Psi_+] - iS[\Psi_-] + i\int dt \, (J_+\Psi_+ - J_-\Psi_-) \Big), \tag{99}$$

where $\Psi_\pm$ collectively denotes all system, apparatus, and bath fields on the forward/backward branches, $S[\Psi]$ is the microscopic action corresponding to Eq. (98), and $J_\pm$ are source fields. The doubling of fields—the hallmark of the Keldysh formalism—encodes the initial density matrix and ensures the correct causal structure for real-time correlation functions [24].

It is convenient to introduce the classical and quantum Keldysh rotations:

$$\Psi_{\text{cl}} = \tfrac{1}{2}(\Psi_+ + \Psi_-), \qquad \Psi_q = \Psi_+ - \Psi_-. \tag{100}$$

In this basis, $\Psi_{\text{cl}}$ corresponds to physical (retarded) response and $\Psi_q$ to noise (fluctuation) degrees of freedom. The causality structure of the theory is manifest: the retarded Green's function couples $\Psi_q$ to $\Psi_{\text{cl}}$, while the Keldysh component (noise) couples $\Psi_q$ to $\Psi_q$.

## C.3 Integrating Out Fast Modes

The derivation proceeds by systematically eliminating degrees of freedom that are fast compared to the collective order parameter $\Phi$.

**Step 1: Mode decomposition.** The apparatus operators are separated into slow (collective) and fast (individual fluctuation) components:

$$\hat{A}_i = \hat{A}_i^{(s)} + \hat{A}_i^{(f)}, \qquad \text{with} \quad \Phi = \frac{1}{\sqrt{N}} \sum_{i=1}^N \hat{A}_i^{(s)}, \tag{101}$$

where $\hat{A}_i^{(s)}$ projects onto modes with frequencies below the coarse-graining cutoff $\Lambda$ and $\hat{A}_i^{(f)}$ captures the remainder. This separation is the standard Wilsonian decomposition applied to the apparatus field.

**Step 2: Integrating out the bath.** The bath degrees of freedom are Gaussian (or treated as such in the weak-coupling limit). Performing the Gaussian path integral over the bath fields yields the influence functional [25]:

$$e^{iS_{\text{IF}}[\Phi_+, \Phi_-]} = \int \mathscr{D}[\text{bath}] \; \exp(iS_{\text{bath}} + iS_{A\text{-bath}}[\Phi_\pm, \text{bath}]) \, . \tag{102}$$

The influence functional contributes two kernels to the effective action for $\Phi$:

$$\text{Dissipation kernel:} \quad \mathscr{D}(t-t') = \text{Im}\big[\langle \hat{B}(t)\hat{B}(t')\rangle_{\text{bath}}\big] \, , \tag{103}$$

$$\text{Noise kernel:} \quad \mathscr{N}(t-t') = \text{Re}\big[\langle \{\hat{B}(t), \hat{B}(t')\}\rangle_{\text{bath}}\big] \, , \tag{104}$$

where $\hat{B}$ is the bath operator coupled to $\Phi$ in $\hat{H}_{A\text{-bath}}$. These kernels satisfy the fluctuation-dissipation relation at temperature $T$:

$$\mathscr{N}(\omega) = \coth\left(\frac{\omega}{2k_B T}\right) \mathscr{D}(\omega). \tag{105}$$

**Step 3: Integrating out fast apparatus modes.** The fast modes $\hat{A}_i^{(f)}$ are integrated out via a cumulant expansion. At Gaussian order, they renormalize the coefficients of $\Phi$ in the effective action (mass renormalization, stiffness renormalization). At quartic order, they generate the $\Phi^4$ interaction vertex—this is the microscopic origin of the quartic term in the Landau potential.

**Step 4: Integrating out system degrees of freedom.** In the measurement regime, the system evolves on timescales fast compared to the macroscopic pointer relaxation ($\tau_S \ll \tau_{\text{pointer}}$). The system path integral is therefore performed with $\Phi$ held fixed, yielding an effective potential:

$$V_{\text{sys}}[\Phi] = -\frac{1}{\beta_{\text{eff}}} \ln \text{Tr}_S \exp\Big( -\beta_{\text{eff}} \hat{H}_S - \beta_{\text{eff}} g \hat{S} \sqrt{N} \Phi \Big) \, , \tag{106}$$

where $\beta_{\text{eff}}^{-1} = k_B T_{\text{eff}}$ is set by the system's effective temperature. For a two-level system with $\hat{S} = \hat{\sigma}_z$, this evaluates to:

$$V_{\text{sys}}[\Phi] = -\frac{1}{\beta_{\text{eff}}} \ln\Big[ 2\cosh\Big( \beta_{\text{eff}} g \sqrt{N} \Phi \Big) \Big] \, . \tag{107}$$

Expanding to quartic order: $V_{\text{sys}} \approx -g^2 N \Phi^2/2 + g^4 N^2 \Phi^4/12 + \cdots$, which contributes the symmetry-breaking quadratic and stabilizing quartic terms.

### C.4 Effective Action for $\Phi$

After all integrations, the effective Keldysh action for the collective coordinate $\Phi_{\rm cl}, \Phi_q$ (in the classical/quantum basis) takes the form:

$$S_{\rm eff}[\Phi_{\rm cl}, \Phi_q] = \int dt \Big[ \Phi_q \left( i\partial_t \Phi_{\rm cl} + \Gamma \frac{\delta V}{\delta \Phi_{\rm cl}} \right) + i\Gamma k_B T_{\rm eff} \Phi_q^2 + \mathcal{O}(\Phi_q^3) \Big] \quad (108)$$

where $V(\Phi)$ is the total effective potential incorporating contributions from the apparatus self-interaction, the system integration (Eq. (106)), and fast-mode renormalization; $\Gamma$ is the relaxation rate set by the dissipation kernel; and $T_{\rm eff}$ is the effective temperature of the slow mode, related to the noise kernel via Eq. (105).

The structure of Eq. (108) is dictated by general principles:

- The $\Phi_q \cdot \partial_t \Phi_{\rm cl}$ term encodes the retarded (causal) dynamics.
- The $\Phi_q \cdot \delta V / \delta \Phi_{\rm cl}$ term generates the deterministic force.
- The $i\Phi_q^2$ term is the Keldysh (noise) component, generating stochastic fluctuations.
- Higher-order terms $\mathcal{O}(\Phi_q^3)$ encode non-Gaussian noise and are negligible in the semiclassical limit.

### C.5 Saddle-Point Equations and Fluctuations

**Saddle-point (deterministic dynamics).** Setting $\delta S_{\rm eff}/\delta \Phi_q = 0$ yields the equation of motion for $\Phi_{\rm cl}$:

$$\partial_t \Phi = -\Gamma \frac{\delta V}{\delta \Phi}, \quad (109)$$

which is precisely the deterministic TDGL equation (47) with $D = \Gamma$.

**Gaussian fluctuations.** Expanding about the saddle point, the quadratic action in $\Phi_q$ generates Gaussian noise $\eta(t)$ with correlator:

$$\langle \eta(t)\eta(t') \rangle = 2\Gamma k_B T_{\rm eff} \delta(t-t'), \quad (110)$$

recovering the Langevin noise in Eq. (47). The fluctuation-dissipation relation (105) guarantees that the noise amplitude and the dissipation coefficient are related by the effective temperature, ensuring thermodynamic consistency.

### C.6 Coarse-Graining to $\psi$ and Emergence of $\phi^4$

The final step defines the spatially coarse-grained order parameter:

$$\psi(\mathbf{x}, t) = \int d^3y \, f(\mathbf{x}-\mathbf{y}) \, \Phi(\mathbf{y}, t), \quad (111)$$

as in Eq. (17). The effective potential $V(\psi)$ is obtained by collecting all contributions from the cumulant expansion:

$$V(\psi) = a_2 \, \psi^2 + a_4 \, \psi^4 + \mathcal{O}(\psi^6), \quad (112)$$

where the coefficients have explicit microscopic expressions:

$$a_2 = \frac{\lambda}{2}\left(1 - \frac{\gamma}{\gamma_{\rm c}}\right), \qquad \text{with} \quad \gamma = g\sqrt{N}, \quad (113)$$

$$a_4 = \frac{\lambda}{4} > 0. \quad (114)$$

The critical coupling $\gamma_{\rm c}$ is determined by the competition between the apparatus self-energy (which favors $\psi = 0$) and the system-mediated interaction (which favors $\psi \neq 0$). At the critical point, with maximal system polarization ($|\langle \hat{S} \rangle| = \hbar\omega_S$), the condition $\gamma = \gamma_{\rm c}$ becomes:

$$\gamma_{\rm c}^{-1} = g\sqrt{N} = \frac{\text{system–apparatus coupling} \times \sqrt{\text{apparatus size}}}{\text{apparatus self-energy scale}}. \quad (115)$$

This reproduces the scaling $\gamma_{\rm c} \sim (g\sqrt{N})^{-1}$ derived in the main text (Eq. (28)), where $\gamma_{\rm c} = \lambda/(\hbar\omega_S)$ is an apparatus property and the $g$-dependence enters through the coherence pressure $\gamma$ (Eq. (28)).

**Origin of the $\phi^4$ structure.** The quartic term $a_4\psi^4$ arises from two sources: (i) the quartic term in the cumulant expansion of $V_{\rm sys}[\Phi]$ (Eq. (107)), which reflects the saturation of a two-level system; and (ii) the fourth-order cumulant of fast apparatus mode fluctuations, which provides the standard Landau stabilization. Both contributions are strictly positive, ensuring $a_4 > 0$ and hence thermodynamic stability.

**Summary of the derivation chain.** The full path from microscopic Hamiltonian to macroscopic TDGL is:

$$\hat{H} \xrightarrow{\text{Keldysh}} \mathscr{Z} \xrightarrow{\text{bath}} S_{\rm IF} \xrightarrow[+\,\text{system}]{\text{fast modes}} S_{\rm eff}[\Phi_{\rm cl}, \Phi_q] \xrightarrow{\text{saddle}} \text{TDGL}[\psi]$$

Each arrow is a controlled approximation: the Keldysh construction is exact; the bath integration assumes weak system–bath coupling (valid for Markovian environments); the fast-mode integration is a standard Wilsonian RG step; the system integration assumes $\tau_S \ll \tau_{\rm pointer}$ (valid in the measurement regime); and the saddle-point approximation is justified for macroscopic $N$ where quantum fluctuations of $\Phi$ are suppressed by $1/\sqrt{N}$. No step requires modification of the Schrödinger equation.

## D Scaling Relations and Critical Exponents

For the Ginzburg–Landau functional in $d$ dimensions, the critical exponents are:

**Mean-field values** (valid for $d > 4$):

$$\nu = 1/2 \quad \text{(correlation length)} \quad (116)$$

$$\eta = 0 \quad \text{(anomalous dimension)} \quad (117)$$

$$\gamma_{\rm exp} = 1 \quad \text{(susceptibility)} \quad (118)$$

$$z = 2 \quad \text{(dynamical exponent)} \quad (119)$$

The collapse time scales as $\tau_{\rm c} \sim \xi^z \sim |\gamma - \gamma_{\rm c}|^{-\nu z} = |\gamma - \gamma_{\rm c}|^{-1}$.

**Validity of mean-field theory**: Mean-field exponents apply when the effective dimensionality $d_{\rm eff} > 4$. For apparatus with many degrees of freedom, the effective dimensionality is high (each mode contributes a dimension), so mean-field theory is typically valid. Fluctuation corrections become important only for very small $N$ or near special symmetry points.